Lateral sodium diffusion in dendrites of CA1 pyramidal neurons

Laterale Natriumdiffusion in Dendriten von CA1 Pyramidenzellen

Inaugural-Dissertation

zur Erlangung des Doktorgrades
der Mathematisch-Naturwissenschaftlichen Fakultät
der Heinrich-Heine-Universität Düsseldorf

vorgelegt von

Joel Sean Elliot Nelson
aus Düsseldorf

Düsseldorf, Juni 2024

aus dem Institut für Neurobiologie
der Heinrich-Heine-Universität Düsseldorf

Gedruckt mit der Genehmigung der
Mathematisch-Naturwissenschaftlichen Fakultät der
Heinrich-Heine-Universität Düsseldorf

Berichterstatter:

1. Prof. Dr. Christine R. Rose, Heinrich-Heine-Universität Düsseldorf

2. Prof. Dr. Andreas Reiner, Ruhr Universität Bochum

Tag der mündlichen Prüfung: 4.11.2024

“Vivere est cogitare” - "*To live is to think”*

- Marcus Tullio Cicero

Abstract

During glutamatergic synaptic transmission in the vertebrate brain, the influx of sodium ions (Na^+) through ligand-gated ion channels drives the depolarization of the postsynaptic neuron. A fast clearance of Na^+ from its point of entry is crucial for the cell, as prolonged increases in intracellular Na^+ concentrations ($[Na^+]_i$) lead to persistent depolarizations and a breakdown of Na^+-dependent secondary transport processes. Such local dendritic Na^+ increases are mainly cleared via fast lateral diffusion. While it is known that the diffusional dynamics of molecules and ions such as Cl^- are severely slowed, e.g. due anomalous diffusion in spiny dendrites, studies addressing the properties of Na^+ diffusion along dendrites are still lacking. To fill this gap, this study focused on the diffusional dynamics of Na^+ in dendrites of CA1 pyramidal neurons. This study thereby firstly determined $[Na^+]_i$ in dendrites and addressed how it is influenced by neuronal activity. Secondly, this study investigated the spread of Na^+ through the dendrite after local intrusion, also establishing its diffusional characteristics. It thereby considered the impact of dendrite morphology, namely spine density, which has been reported to dampen dendritic diffusion of molecules. Furthermore, this study investigated the ability of Na^+ to cross from the dendrite into neighboring spines, thus addressing spine-dendrite coupling and possible diffusional compartmentation. To this end, fluorescence lifetime imaging (FLIM) of the Na^+-sensitive dye ING-2 combined with whole-cell patch-clamp was performed for the quantitative determination of $[Na^+]_i$ within apical dendrites of CA1 pyramidal neurons in organotypic slices of the mouse hippocampus. Apical dendrites displayed $[Na^+]_i$ of around 9.5 mM which was reduced upon neuronal silencing. This underlines that neuronal signaling leads to transient increases in $[Na^+]_i$ and shows that dendritic $[Na^+]_i$ is shaped by neuronal activity. Furthermore, local glutamate iontophoresis and two-photon Na^+ imaging in the line-scan mode (again combined with whole-cell patch-clamp) was employed to investigate the spread of Na^+. Na^+ diffused along dendrites and invaded adjacent spines, demonstrating rapid diffusional spine- dendrite coupling. The ability of Na^+ to pass into spines was thereby heterogeneous indicating varying degrees of spine compartmentation, which influences the diffusional coupling between dendrites and spines. This study also shows that the apparent diffusion coefficients (D_{App}) of Na^+ which diffused along the dendrite decreased over time starting at around 200-400 $\mu m^2\ s^{-1}$ and decreasing to approximately 50-100 $\mu m^2\ s^{-1}$ after 2 s. This decrease was explainable through normal diffusion and was not dependent on the morphology of the dendrite. This indicates that diffusional characteristics of Na^+ in dendrites are significantly slower than previously reported for cellular structures (600-1300 $\mu m^2\ s^{-1}$). The results are also in contrast to studies which show spine density dependent occurrence of anomalous diffusion in dendrites. Simulation studies show, that dampened Na^+ dynamics have a major impact on the physiology of the neuron. This underlines the importance of the here provided study which provides experimental evidence of $[Na^+]_i$ dynamics in the dendrite.

Zusammenfassung

Der Einstrom von Natriumionen (Na^+) durch ligandengesteuerte Ionenkanäle während der glutamatergen synaptischen Übertragung führt zu einer Depolarisierung der Postsynapse. Eine schnelle Beseitigung von Na^+ von der Eintrittsstelle ist von entscheidender Bedeutung, da erhöhte intrazelluläre Na^+-Konzentrationen ($[Na^+]_i$) zu anhaltenden Depolarisationen und einem Zusammenbruch der gekoppelten sekundären Transportprozesse führen kann. Solche lokalen Na^+ Erhöhungen werden vorwiegend duch laterale Diffusion beseitigt. Während bekannt ist, dass die Diffusionsdynamik von Molekülen und Ionen we Cl^- verlangsamt ist, z. B. durch anomale Diffusion in Dendriten mit Dornfortsätzen (Spines), fehlen bisher Studien, die sich mit den Eigenschaften der Na^+ Diffusion in Dendriten beschäftigen. Um diese Lücke zu schließen, konzentrierte sich diese Studie auf die Diffusionsdynamik von Na^+ in Dendriten von CA1- Pyramidalneuronen. Dafür wurde zunächst $[Na^+]_i$ in Dendriten bestimmt und untersucht, wie es durch neuronale Aktivität beeinflusst wird. Desweiteren wurde die Ausbreitung von Na^+ innerhalb des Dendriten untersucht, wobei dessen Diffusionseigenschaften ermittelt wurden. Dabei wurde die Auswerkung der Dendritenmorphologie, d.h. der Spine-Dichte, berücksichtig, von der berichtet wurde, dass sie die dendritische Diffusion von Molekülen dämpft. Darüber hinaus wurde in dieser Studie untersucht, ob Na^+ in der Lage ist von Dendriten in Spines zu diffundieren. Zu diesem Zweck wurde Fluoreszenz- Lebensdauer- Imaging (FLIM) des Na^+ sensitiven Farbstoffs ING-2 in Kombination mit Ganzzell-Patch-Clamp zur quantitativen Bestimmung von $[Na^+]_i$ in apikalen Dendriten von CA1-Pyramidalneuronen in organotypischn Schniten des Maus Hippocampus durchgeführt. Dendriten wiesen eine $[Na^+]_i$ von etwa 9.5 mM auf, der durch das Ausschalten neuronaler Aktivität reduziert wurde. Dies unterstreicht, dass neuronale Signale zu einem transienten Anstieg von $[Na^+]_i$ führt und zeigt, dass dendritische $[Na^+]_i$ durch neuronale Aktivität beeinflusst wird. Darüber hinaus wurden Glutamat-Iontophorese und Zwei Photonen Na^+ Bildgebung im Line- Scan- Modus (wiederum in Kombination mit Ganzzell- Patch- Clamp) eingesetzt, um die Ausbreitung von Na^+ zu untersuchen. Na^+ diffundierte innerhalb der Dendriten und in anliegende Spines, was eine schnelle diffusionelle Kopplung zwischen Spines und Dendriten zeigt, welche heterogen war. Die Daten deuten also auf einen unterschiedlich Grad der Spine-Kompartmentieung hin, welcher die Diffusion beeinflusst. Diese Studie zeigt auch, dass die gemessenen Diffusionskoeffizienten (D_{App}) von Na^+, welches entlang des Dendriten diffundierten, über 2 Sekunden von 200-400 $\mu m^2\ s^{-1}$ auf 50-100 $\mu m^2\ s^{-1}$ abnahmen. Dieser Rückgang war durch normale Diffusion erklärbar und hing nicht von der Morphologie des Dendriten ab. Dies zeigt zum einen, dass die Diffusionseigenschaften von Na^+ in Dendriten deutlich langsamer sind, als bisher für cellulären Strukturen berichtet wurde (600-1300 $\mu m^2\ s^{-1}$). Darüber hinaus deuten die Daten darauf hin, dass die Dämpfung der Na^+- Diffusionsdynamik nicht von der Morphologie der Dendriten abhängt, was im Gegensatz zu Studien steht , die eine von der Spinedichte abhängige anomale Diffusion zeigen. Studien, welche die langesame diffusion von Na^+ simulieren zeigen, dass langsame Dynamiken große Implikationen für die Physiologie des Neuons haben. Dies unterstreicht die Bedeutung der hier vorgelegten Studie, die den expermentellen Nachweis der Na^+ Dynamik im Dendriten lefert.

Content

Preface

This work is committed to the understanding of sodium (Na^+) dynamics in the dendritic tree. To enable an in-depth understanding about the relevance of the topic, this work will firstly introduce key aspects related to the dynamics of Na^+ in spiny dendrites.

As such, this thesis introduces the CA1 pyramidal neuron describing its distinct morphology and function as information processing unit. It then explains the functionality of the CA1 neuron, as its function is dependent on specific ion gradients and is relies on the opening of ion channels. This study thereby focuses on the impact of Na^+ on the neuron, emphasizing the importance for a strict regulation of the intracellular Na^+ concentration ($[Na^+]_i$). It then describes glutamatergic synaptic transmission as a key process for Na^+ intrusion and points out the important role of diffusion-mediated Na^+ clearance from its intrusion site. Moreover, this thesis unrolls the rules and processes, which underline diffusion within the dendrite, emphasizing characteristics which may impact diffusion of compounds and ions, such as Na^+. Finally, this work provides an overview about the morphological characteristics of spines including their general morphology and compartmentation characteristics.

Taken together, this introduction will outline the need to understand Na^+ dynamics in dendrites, emphasize the influence of Na^+ diffusion after synaptic transmission and discuss the effects of morphological characteristics on its intracellular diffusion.

1. Morphology of the pyramidal neuron

1.1 The connectivity of the brain

Among all organs within the body, the vertebrate brain holds a special role, as it governs the function of the other organs, the movement of the body, but also consciousness, memory and character of the animal. Research has been pushing to understand the brain on a global, on a network, a cellular, and a subcellular level (Sporns, 2011; Bardin, 2012; Pessoa, 2014; Yates and Scholl, 2022; Ishikawa et al., 2023). The complexity of the brain itself is difficult to fathom, as it is built up of a multitude of different interconnecting brain regions (Fig. 1) which are responsible for different tasks. These regions display defined networks of specific interconnecting cells which allow the network to function. Neuronal cells essentially enable the computation and transmission of signals. Although brain function is shaped by the collaboration of many different cell types, neurons are the cells which are electrically excitable and act as signal processing units. As such, neurons receive signals from other neurons through intercellular connections termed synapses and relay the processed information

through their axon. The number of neurons in the human brain has been estimated at around 85 billion (Williams and Herrup, 1988), with each neuron forming tens of thousands of synaptic connections. These numbers underline the complexity of the connectivity and the processing power of the brain. A subset of neurons termed pyramidal neurons are primarily found in structures that are associated with advanced cognitive functions, for example in the cerebral cortex, the amygdala and the hippocampus (Spruston, 2008). The understanding of these pyramidal neurons, which are named after the triangle shape of their cell body (soma), is necessary for the understanding of such sophisticated functions as learning and memory, as they display characteristics which are key for such processes. Therefore, decades of research have been invested in the understanding of pyramidal neurons, which underlying function as signal processing unit is resembled in its morphological features.

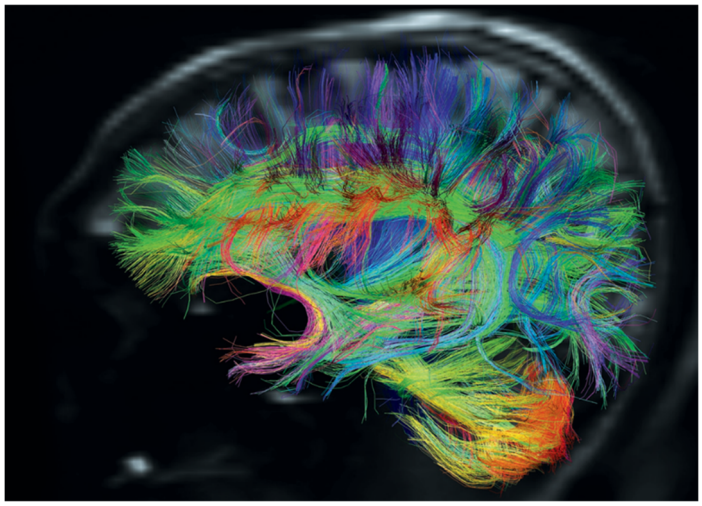

Figure 1: Neuronal connections in the brain. Image of the web of nerve fiber bundles (the "connectome") which interconnects different regions within the human brain. Taken from (Bardin, 2012).

1.2 The morphological properties of pyramidal neurons

The pyramidal neuron is typically composed of soma, both basal and apical dendritic trees and an axon (Fig. 2 A) (Harris et al., 2001). As mentioned before, pyramidal neurons are abundantly dispersed throughout a multitude of brain areas and are also allocated within the CA1 region of the hippocampus. The soma of CA1 pyramidal neurons is located in the *stratum pyramidale*, with basal dendrites extending into the *stratum oriens* and apical dendrites extending through the *stratum radiatum* and into the *stratum lacunosum moleculare*, where they branch into an apical turft (Bannister and Larkman, 1995a). The arborization of the dendritic tree is classified into several orders, depending on the extent of ramification. Dendrites that originate from the soma are classified as primary dendrites. Dendrites that branch out from the primary dendrite are called secondary dendrites, with further ramifying dendrites declared as tertiary dendrites (Fiala and Harris, 1999; Langhammer et al., 2010; Holmes and Berkowitz, 2014; O'Neill et al., 2015; Tian et al., 2022). The morphology of the pyramidal neuron is similar to its function as a signal processing unit, as dendrites receive signals from other neurons through synapses. The incoming information is then transmitted to the soma and processed (Magee, 2000). If the sum of incoming signals is large enough, an

action potential is generated at the axon hillock (Colbert and Johnston, 1996; Golding and Spruston, 1998) and projects through the axon to contact the dendrites of other receiving neurons.

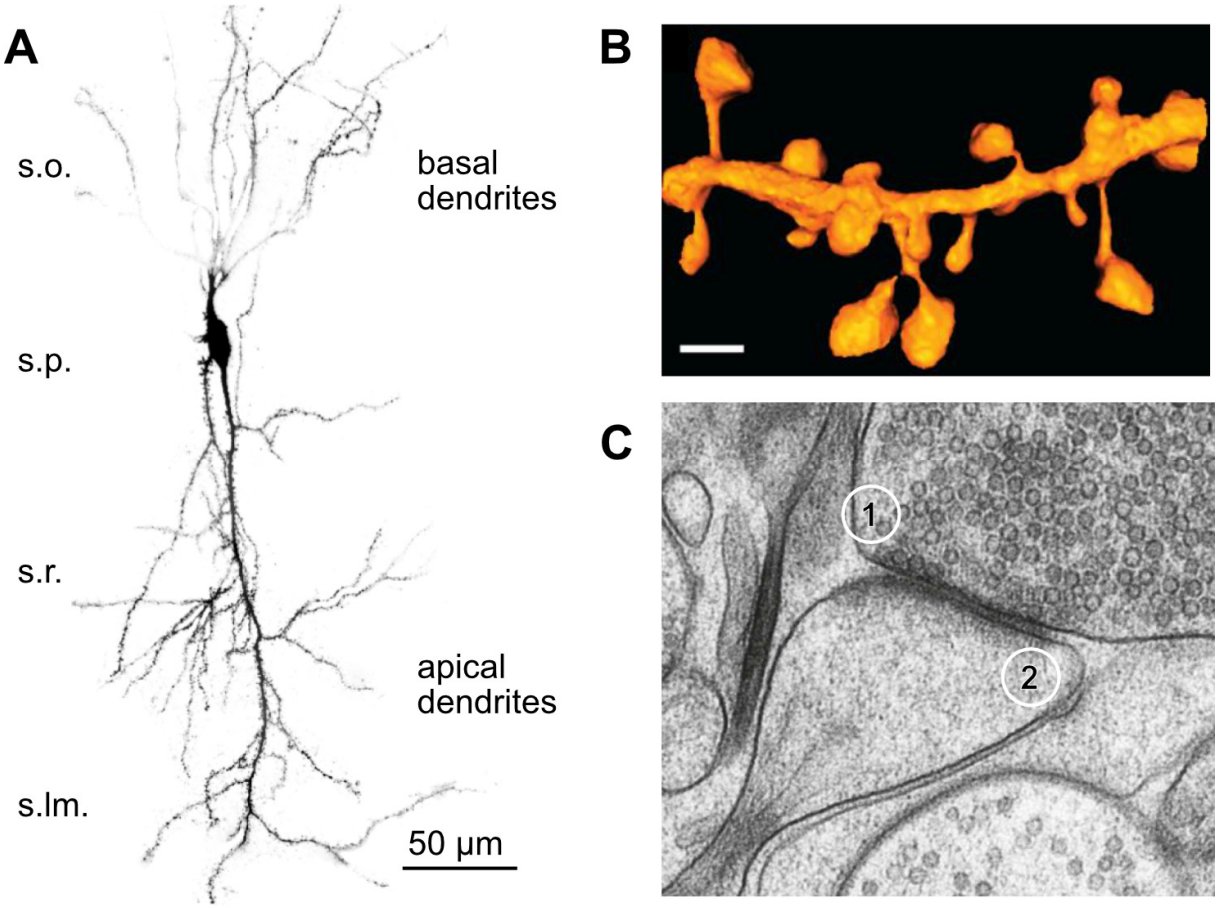

Figure 2: The morphology of a CA1 pyramidal neuron A: Image of a CA1 pyramidal neuron individually loaded with the Na^+ sensitive dye Na^+-binding benzofuran isophosohthalate (SBFI). Layers of the CA1 region as *stratum oriens* (s.o.), *statum pyramidale* (s.p.), *stratum radiatum* (s.r.) and stratum *lacunosum moleculare* (s.lm.). Soma, as well as basal and apical dendrites are labelled. (Nelson JSE., unpublished). **B**: Stimulated emission depletion (STED) microscopy image of a dendritic segment which carries multiple spines. Spine heads are connected to the dendrite through the spine neck. The scale bar is 1 µm. Taken from (Tønnesen and Nägerl, 2016). **C**: Electron microscopic image of a synapse with the presynaptic terminal (1) and the postsynaptic spine (2). Vesicles are visible in the presynapse, whereas the spine includes the spine neck, spine head and the postsynaptic density. Modified from (Korogod et al., 2015).

The dendrites of pyramidal neurons are covered with small micron sized protrusions termed spines (Peters and Kaiserman-Abramof, 1970; Harris et al., 2001) (Fig. 2 B). These are identified as the postsynaptic sites of glutamatergic synapses, which are a defining characteristic for pyramidal neurons (DeFelipe and Fariñas, 1992; DeFelipe, 2011). Spines have a typical morphology comprised of a spine head and a spine neck, connecting the head to the dendrite (Gray, 1959; Korogod et al., 2015) (Fig. 2 C). The spine head carries the postsynaptic density, which incorporates various proteins, including glutamate receptors and anchor proteins (Swulius et al., 2010). The number of spines is dependent on the surrounding synaptic input, which facilitates spine motility and growth (Das et al., 1998; Engert and

Bonhoeffer, 1999; Maletic-Savatic et al., 1999; Ultanir et al., 2007). As such, spine density represents the minimum estimate of the rough number of excitatory synaptic inputs onto the neuron for a certain dendritic segment (Segal and Andersen, 2000).

The organization of spines is thereby highly regulated and dependent on the dendrite order, synaptic input and also dendritic diameter (Parajuli et al., 2020). As spine numbers have been estimated at 23,000-34,800 spines per cell (Andersen, 1990; Bannister and Larkman, 1995b; Megıas et al., 2001; Konur et al., 2003), the synaptic connections between pyramidal neurons is unfathomable. Studies have also shown, that computation of synaptic signals occurs at the spine level, leading to the reshaping of the spine's morphology. As such spines are recognized as the smallest computational unit of the neuron (Harris and Kater, 1994; Shepherd, 1996).

Therefore, if we aspire to understand the functions of the brain and its pathways. We must also understand the function of not only a single neuron, but of a dendrite with its spines, as well as the processes which occur within a single spine. Such processes are based in the dynamics of specific ions, which enable neuronal functioning.

2. The role of Na^+ for the neuron

2.1. The importance of the inward directed Na^+ gradient

The electrochemical characteristic of the neuron is based on specific ion gradients, which are established through defined ion concentrations within the cell and in the extracellular space (Fig. 3). Potassium (K^+) for example is kept at high intracellular concentrations (145 mM), although extracellular concentrations are low (2.5 mM), resulting in an outward-directed chemical gradient. $[Na^+]_i$ on the other hand is kept in low concentrations in the cell (8-15 mM) (Rose and Ransom, 1997; Karus et al., 2015; Mondragão et al., 2016; Meyer et al., 2022) while displaying large extracellular concentrations (around 145 mM) (Harrington et al., 2010), which results in an inward-directed electrochemical gradient. The distribution of ions, among them Na^+, Cl^- and K^+, and their respective permeability, define the membrane potential of the cell. The Goldman-Hodgkin-Katz equation (Goldman, 1943; Hodgkin and Katz, 1949; Hille, 2011) (Eq. 1) describes the membrane potential (E_m) using the permeability (P) and the intracellular and extracellular concentration ([ion]) of the major ions.

$$E_m = \frac{RT}{F} \ln \frac{P_{Na}[Na^+]_{out} + P_K[K^+]_{out} + P_{Cl}[Cl^-]_{in}}{P_{Na}[Na^+]_{in} + P_K[K^+]_{in} + P_{Cl}[Cl^-]_{out}} \qquad \text{(Eq. 1)}$$

As such, the extra- and intracellular ion compositions are of importance and highly specific. The resting membrane potential of pyramidal neurons is typically around -60 to -70 mV (Golding et al., 2005), whereupon changes in the permeability, mostly through the opening

and closing of ion channels, result into a shift in potential. As such, the opening of K^+ channels lead to an efflux of K^+ with accompanying hyperpolarization of the cell membrane. The opening of Na^+ channels has the opposite effect with Na^+ following its electrochemical gradient into the cell which results in the depolarization of the cell membrane. Due to its depolarizing effect, Na^+ is recognized as the main excitatory charge carrier. The influx of Na^+ is crucial in a number of signaling processes, such as the triggering of excitatory postsynaptic potentials (EPSPs) after synaptic transmission and the generation of APs at the axon hillock (Golding and Spruston, 1998; Umemiya et al., 1999).

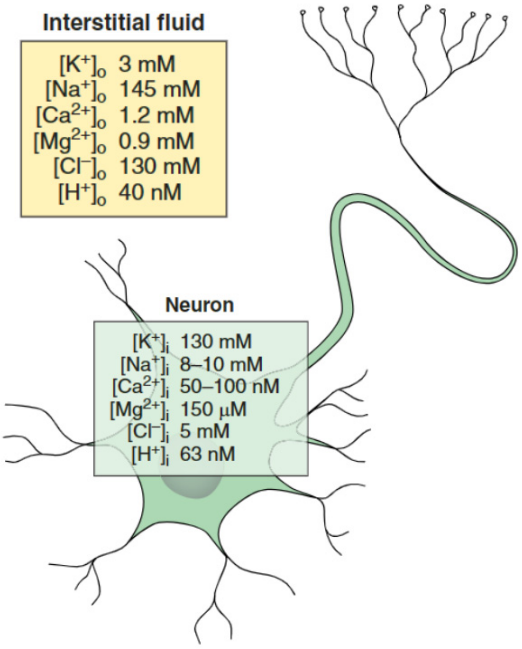

Figure 3: Intra and Extracellular ion compositions. Schematic overview of ion compositions in the neuron, as well as the extracellular space. Taken from (Verkhratsky and Nedergaard, 2018).

The inward directed Na^+ gradient is also used as an energy source to enable secondary transport processes across the cell membrane (Fig. 4). As such, a number of transporters are dependent on the Na^+ gradient to transport neurotransmitters, for example glutamate or gamma-aminobutyric acid (GABA) across the astrocytic membrane, removing them from the synaptic cleft (Kirischuk et al., 2012). Furthermore, other ions such as K^+, Protons (H^+) or calcium (Ca^{2+}) are also transported using the Na^+ across the cell membrane of neurons and astrocytes (Kirischuk et al., 2012). The Na^+-Ca^{2+} exchanger (NCX) for example, uses the Na^+ gradient to transport Ca^{2+} out of the cell (Matsuoka et al., 1997; Blaustein, 2010). The regulation of $[Ca^{2+}]_i$ is critical and must be kept at low intracellular concentrations due to its functions as a second messenger (Hardingham and Bading, 1999). However, the transport via the NCX is heavily dependent on the Na^+ gradient and the depolarization of the cell membrane, also switching into the reverse mode in cases of high $[Na^+]_i$ as a way to extrude Na^+ out of the cell (Philipson and Nicoll, 2000; Dietz et al., 2007; Gerkau et al., 2017b; Oschmann et al., 2017; Ziemens et al., 2019).

In summary, Na^+, the main excitatory charge carrier follows its gradient into the cell as Na^+ channels open. This leads to depolarization of the cell membrane and signaling events. However, Na^+ not only leads to the depolarization of the cell membrane, it is also heavily involved in the intracellular maintenance and transport of other compounds, as the Na^+ gradient is coupled to a large number of other secondary transport processes. The maintenance of low $[Na^+]_i$ is therefore crucial for the functionality of the cell and assured through the activity of the

Na^+-K^+-ATPase (NKA) (Rose and Ransom, 1997; Azarias et al., 2013). Prolonged accumulation of Na^+ has serious consequences for the cell ranging from severe depolarization to collapse of the Na^+ gradient. The breakdown of the Na^+ gradient also leads to an impairment of other ion gradients. Because of its importance, $[Na^+]_i$ dynamics have been studied for decades using methods such as dynamic imaging with fluorescent Na^+ sensors (Rose, 1997; Rose and Ransom, 1997) or Na^+-sensitive microelectrodes (Deitmer and Ellis, 1980). Studies have focused on Na^+ dynamics under physiological and pathophysiological conditions and have identified key processes for Na^+ entry (Rose and Konnerth, 2001; Gerkau et al., 2017b; Miyazaki and Ross, 2017; Ziemens et al., 2019). In addition to the investigation of transient changes in $[Na^+]_i$, a great deal of work has been devoted to the determination of $[Na^+]_i$ under resting conditions (baseline $[Na^+]_i$). Until recently, the measurement of such baseline concentrations was limited to the cell soma (Karus et al., 2015; Mondragão et al., 2016; Ziemens et al., 2019). However, determination of dendritic $[Na^+]_i$ has not yet been performed. As dendrites are heavily subjected to synaptic signaling and associated shifts in intracellular ion concentrations, the determination of dendritic $[Na^+]_i$, as well as the influence of synaptic transmission on dendritic $[Na^+]_i$, is of great interest.

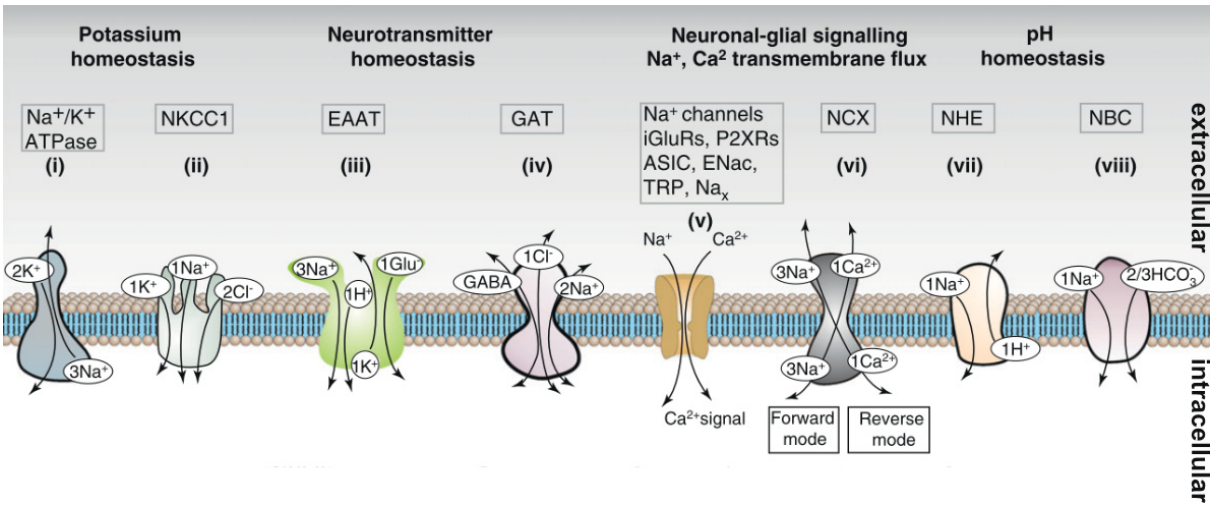

Figure 4: Secondary transport processes which are coupled to the Na^+ gradient. Schematic overview of secondary active transport processes, which use the Na+ gradient for the transport of other compounds across the cell membrane. These include ions such as K+, Ca2+, H+ and bicarbonate, as well as transmitters such as glutamate and GABA. Taken from (Kirischuk et al., 2012).

2.2 Na^+ influx during glutamatergic transmission

In pyramidal neurons, one major pathway for Na^+ to enter the cell occurs during synaptic transmission. During such transmission, information is passed from one neuron to another through the synapse where neurotransmitters are utilized for the transfer of electrochemical signals. The glutamatergic synapse is characteristic for pyramidal neurons. It consists of the presynapse of the sending neuron, the postsynapse of the receiving neuron,

and astrocytic processes, which led to the term “tripartite synapse” (Araque et al., 1999) (Fig. 5).

During synaptic transmission, depolarization of the presynapse leads to the influx of Na^+ through Tetrodotoxin (TTX)- sensitive voltage dependent Na^+ channels (Müller and Somjen, 2000) (Fig. 5 (1)). The Na^+ driven depolarization of the presynaptic terminal leads to the opening of voltage dependent Ca^{2+} channels. This leads to the influx of Ca^{2+} into the presynapse, which induces the release of glutamate into the synaptic cleft. Once glutamate crosses the synaptic cleft and reaches the postsynaptic site it binds to glutamatergic receptors which are embedded in the postsynaptic membrane (Fig. 5 (2)). Key receptors in glutamate signal transmission are the ionotropic glutamate receptors α-amino-3-hydroxy-5-methyl-4-isoxazolpropionic acid receptors (AMPARs) and N-methyl-D-aspartate receptors (NMDARs) (Watt et al., 2000). Such receptors open upon the binding of glutamate which enables the influx of Na^+ into the post synapse (Rose and Konnerth, 2001; Miyazaki and Ross, 2017; Ziemens et al., 2019; Miyazaki and Ross, 2022). This leads to a postsynaptic depolarization which is called EPSPs (Fig. 5 (3)). As such, glutamate is considered to be the primary excitatory transmitter in the brain.

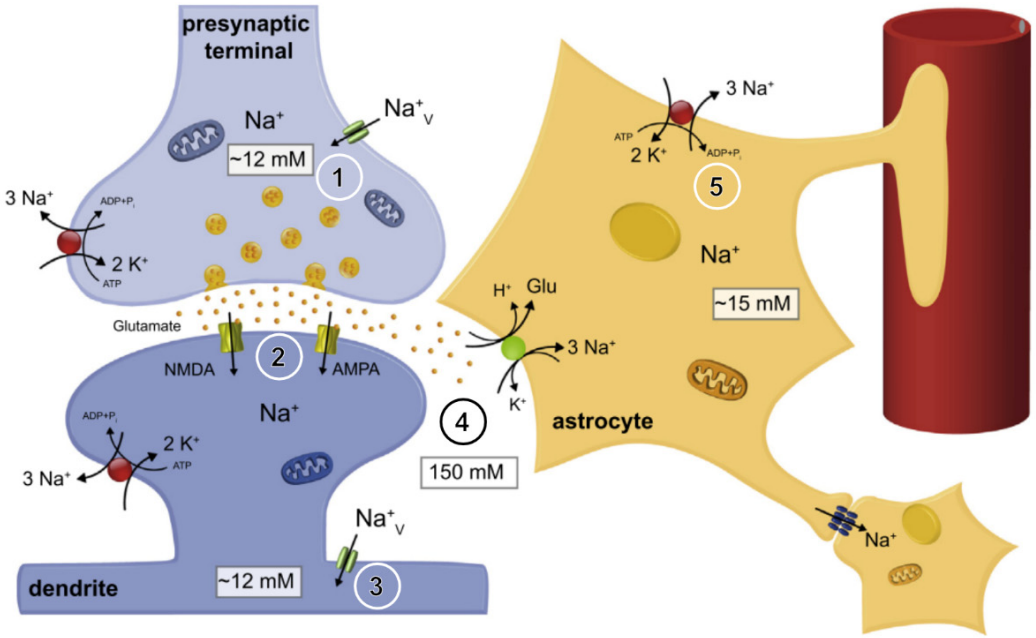

Figure 5: Na^+ dynamics in the tripartite synapse during synaptic transmission. Schematic overview of the tripartite synapse, including the presynaptic terminal, the postsynaptic spine with adjacent dendrite and the astrocyte. Na^+ influx occurs in all components of the synapse, following its inward directed gradient. (1) After depolarization of the presynaptic terminal through an influx of Na^+, glutamate is released into the synaptic cleft. (2) Subsequently, AMPARs and NMDARs are opened upon the binding of glutamate, enabling the influx of Na^+ into the postsynapse. (3) The following depolarization leads to the opening of voltage dependent Na^+ channels (Na^+_V), which ensures further Na^+ influx. (4) The uptake of glutamate out of the synaptic cleft is assured through glutamate transporters, which also co-transport Na^+ and H^+, whilst excluding K^+. (5) Na^+ extrusion out of the cell is facilitated through the Na^+-K^+ ATPase, which is prevalent in all three cells. Modified from (Rose and Chatton, 2016).

Conductance through AMPARs and NMDARs differ significantly (Spruston et al., 1995). While glutamate leads to direct opening of AMPARs, resulting in fast Na^+ intrusion into the post synapse (Miyazaki and Ross, 2017), influx via NMDARs is prevented by a magnesium block (Sah et al., 1989; Kupper et al., 1998). Rapid desensitization of AMPARs limits Na^+ entry and EPSP generation (Ballerini et al., 1995). However, due to the depolarization of the postsynaptic membrane, magnesium is released from the NMDARs pore (Calabresi et al., 1992), allowing further Na^+ influx and stronger depolarization of the postsynapse (Watt et al., 2000). In addition, NMDARs are permeable to Ca^{2+}, allowing its influx into the post synapse (Schiller et al., 1998; Schiller et al., 2000; Schiller and Schiller, 2001; Bloodgood et al., 2009). The influx of Ca^{2+} can lead to secondary processes that result in the recruitment of additional AMPARs into the post synaptic density (PSD) of the receiving spine (O'Brien et al., 1998; Malinow and Malenka, 2002);. This results in stronger $[Na^+]_i$ transients and depolarizations during recurrent synaptic transmission (Schiller and Schiller, 2001). Thus, NMDAR conductance leads to a change in synaptic composition including a change in PSD composition. Due to the dependence on NMDAR activation, such a change in composition is strongly dependent on the degree of synaptic transmission. The ability of the synapse to change depending on the level of activity is called synaptic plasticity and is a key feature of glutamatergic synapses.

After release into the synaptic cleft, it is imperative that glutamate is removed in a fast manner, as extended activation of the glutamate receptors leads to a prolonged Na^+ influx, which in turn leads to long periods of depolarization and can result in Ca^{2+} mediated excitotoxicity (Choi and Rothman, 1990; Lee et al., 1999). The removal of glutamate out of the synaptic cleft is mainly due to glutamate transporters (excitatory amino acid transporters (EAATs) which are expressed in perisynaptic processes of astrocytes (Danbolt, 2001). Thus, astrocytes are key for the uptake of glutamate from the synaptic cleft (Hertz, 1979) (Fig. 5 (4)), not only protecting the neuron from overexcitation, but also enabling the synapse to return to a state, in which new synaptic transmission can occur again. Further research over the last decades revealed that the astrocytes shape the spread of glutamate during synaptic transmission, thereby modulating the degree of synaptic transmission and determining the fate of the synapse (Piet et al., 2004; Haber et al., 2006; Bernardinelli et al., 2011).

In summary, receptors open during glutamatergic synaptic transmission which allows the influx of Na^+ into the post synapse. This leads to the depolarization and the generation of an EPSP. The correct functioning of the tripartite synapse is essential for neuronal physiology. To allow a fast return to ion homeostasis, processes must enable the clearance of $[Na^+]_i$, which enters during synaptic transmission. Such a clearance is imperative for the synapse and effective synaptic transmission.

2.3 NKA vs. lateral diffusion

The extrusion of Na^+ once it has entered the cell is facilitated by the Na^+-K^+ ATPase, which uses ATP to transport Na^+ and K^+ out and into the cell, respectively, against their concentration gradients. As such, regulation of $[Na^+]_i$ is largely dependent on the activity of the NKA (Rose and Ransom 1997; Azarias 1998). It is the disruption of the ATP supply and subsequent shutdown of NKA that leads to an increase in $[Na^+]_i$ during ischemic stroke (Gerkau et al., 2017b; Gerkau et al., 2017a; Pape and Rose, 2023), demonstrating the importance of NKA-mediated regulation of $[Na^+]_i$. As spines and dendrites are subjected to synaptic transmission and thereby a large degree of Na^+ intrusion, fast $[Na^+]_i$ clearance is important to assure the ability for fast recovery after a signaling event. Publications involving labeling of NKA subunits in primary neuronal cultures show prominent staining in the membrane of the dendritic tree and spines (Blom et al., 2011; Liebmann et al., 2013; Blom et al., 2016; Ilouz et al., 2017) (Fig. 6 A). This postulates that NKA-mediated $[Na^+]_i$ extrusion occurs in both dendrites and spines.

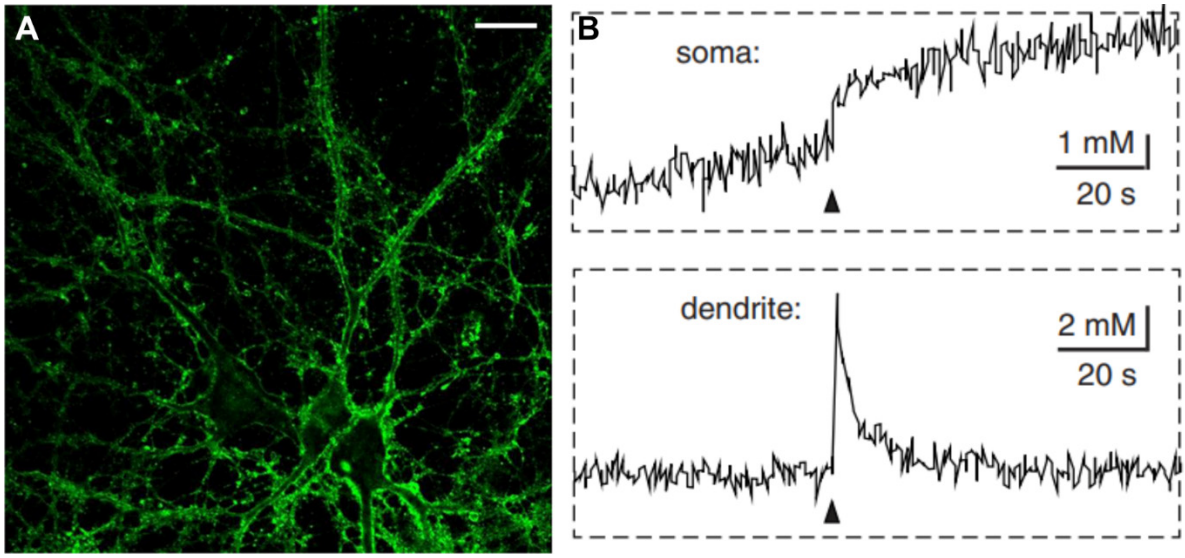

Figure 6: The importance of diffusion for the clearance of local $[Na^+]_i$ elevations. A: Immunofluorescent image of an immunohistochemical NKA staining showing that the NKA is predominantly expressed in the cell membrane of the soma, dendrite and in the spine. Taken from (Blom et al., 2016). **B**: Traces showing glutamate mediated $[Na^+]_i$ signals, as glutamate was applied onto either the soma or the dendrite of a CA1 pyramidal neuron. Experimental conditions involved the blocking of the NKA through the antagonist ouabain. Glutamate application at the soma led to a persistent increase of $[Na^+]_i$, whilst measurements take from dendrites showed a return to baseline. Taken from (Mondragão et al., 2016).

However, previous work has also shown that, while recovery from global $[Na^+]_i$ increases is critically dependent on the activity of the NKA, recovery from local $[Na^+]_i$ increases in dendrites and axons is predominantly mediated by lateral diffusion of Na^+ away from the point of intrusion (Mondragão et al., 2016) (Fig. 6 B). Such studies have shown that blocking the NKA has no effect on the spatiotemporal recovery of local $[Na^+]_i$ increases in the dendrite

which is in contrast to global increases in the soma (Mondragão et al., 2016). Furthermore, Na^+ intrusions mediated by brief, local glutamate applications did not result in a change in intracellular ATP concentrations, suggesting that NKA mediated extrusion of Na^+ plays a minor role in the recovery of the signal. On the other hand, prolonged glutamate applications facilitated large $[Na^+]_i$ signals throughout the dendritic tree and concomitant ATP depletion which suggests an increased activation of the NKA during long, global events (Gerkau et al., 2019). Thus, local Na^+ intrusion, which occur in dendrites during synaptic transmission are cleared by fast lateral diffusion, rather than the comparatively slower NKA mediated extrusion (Mondragão et al., 2016; Miyazaki and Ross, 2022; Canepari and Ross, 2024).

Thus, the role of diffusion along the dendrite is not to be underestimated, as it enables clearance of ions like Na^+ which leads to a fast $[Na^+]_i$ recovery after local synaptic transmission. It is therefore diffusion, which is responsible for the exceedingly fast synaptic signaling capability. As such, understanding of $[Na^+]_i$ dynamics during and after synaptic transmission must incorporate the understanding of ion diffusion throughout the dendrite.

3. Diffusion in the dendritic tree

As diffusion is of such importance for the clearance of local Na^+ intrusions, its dynamics must be considered to understand dendritic processes underlying regulation of the intracellular ion composition, computation of incoming signals and the modulation of dendrites and even spines. Thus, one must understand the basic principles of diffusion, the general diffusional characteristics of ions such as Na^+ and proposed characteristics, which influence the movement of Na^+ away from normal toward anomalous diffusion.

3.1 The laws of diffusion

Diffusion itself has been a subject of interest for the past and describes a process by which molecules move along a concentration gradient as a result of random molecular motion century (Fick, 1855; Crank, 1979; Einstein, 2005). It can be illustrated by a simple experiment, which involves the dropping of colored liquid into clear water. Whilst the coloration of the liquid is very locally confined in the beginning of the experiment, the whole solution appears uniformly colored after sufficient time has passed. As such, the molecules responsible for the coloration have diffused throughout the water from regions of high concentration to regions of low concentration until they are distributed in a homogeneous way. During local increases in the dendrite, Na^+ diffuses along its spatial gradient through the dendrite away from the point of intrusion (Miyazaki and Ross, 2017). As described, this process is essential for the clearance of $[Na^+]_i$ from its point of entry along the dendrite.

The mathematical principles which describe diffusional movement were recognized by (Fick, 1855) and were thereby termed Fick's laws. These state that the diffusive mass flux J at a location x is dependent on the concentration gradient of the molecule (dC/dx), postulating that the flux goes from regions of high concentration to regions of low concentration (Eq. 2).

$$J(x) = -D\frac{dC}{dx} \qquad \text{(Eq. 2)}$$

Where D is the diffusion coefficient, which is a constant of proportionality. The negative sign indicates that diffusion follows its gradient from high to low concentration. Fick´s second law (Eq. 3) is used to predict how diffusion causes the concentration of the molecule to change with respect to the elapsed time (dt), since diffusion proceeds, leading to a change of the gradient. When postulating that the gradient of concentration is only prevalent along the x axis, the resulting one-dimensional diffusion equation results in:

$$\frac{dC}{dt} = -D\frac{d^2C}{dx^2} \qquad \text{(Eq. 3)}$$

This not only postulates the direction of diffusion in one dimension, but also implies that the diffusion speed changes over the length of the dendrite after a local increase, depending on the local concentration gradient. The expression is thereby symmetrical and is represented by a gaussian distribution (Crank, 1979), which decreases in amplitude and increases in width over time (Fig. 7 A). In an experimental setup this is observable when looking at the distribution of an injected substance along one axis over time (Fig. 7 B). Whereas the concentration of the substance is very much confined to the point of injection, it spreads along the axis over time, leading to a decreased amplitude and a wider distribution along the axis.

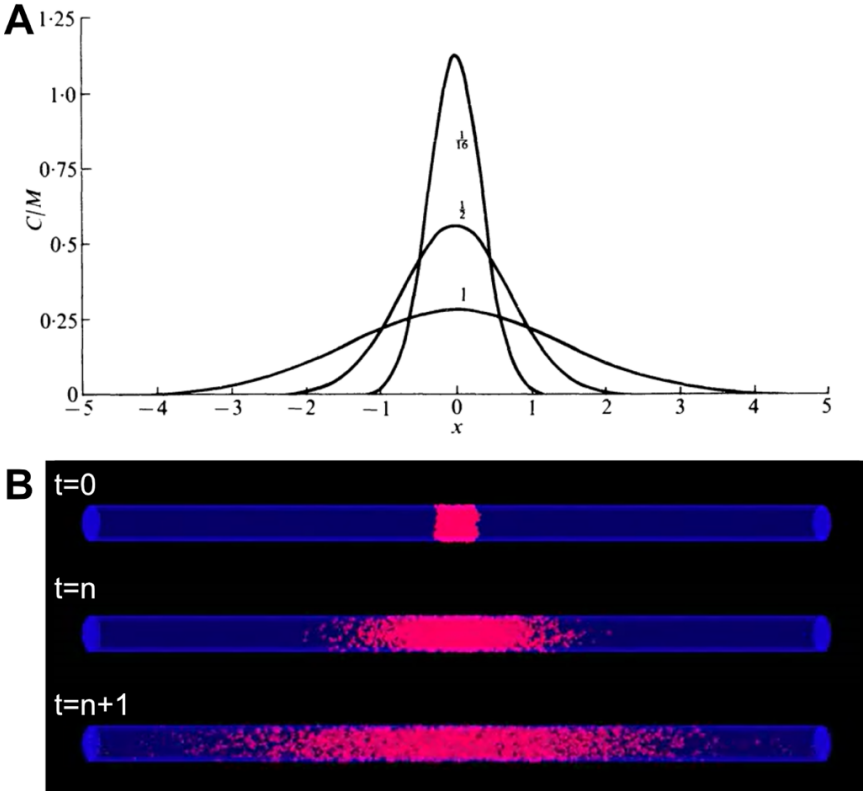

Figure 7: Characteristics of diffusion. A: Gaussian distributions as proposed for concentration distribution in one dimension at different time points. The change of distribution over time follows normal diffusional characteristics. Taken from (Crank, 1979) **B:** Visualization of a change in concentration distribution, which is affected by normal diffusion. Note the tight concentration band at t=0 with a lateral spread of particles with progressing time. Modified from (Mohapatra et al., 2016).

The propagation of a diffusion molecule can be measured by the mean square displacement (MSD), which describes the deviation of a molecule's position from a reference position (x = 0) over time (Fig. 8 A, B). In the case of normal diffusion, the MSD of the diffusing particle is proportional to the Diffusion coefficient *D* and tau τ leading to a linear propagation when plotted as a function over time (MacKintosh, 2012). The MSD ($< r^2 >$) of the solute particle is thereby related to *D* by Eq. 4:

$$< r^2 > = 2D\tau \qquad \text{(Eq. 4)}$$

in one dimension with the diffusion coefficient staying constant over time (Fig. 8 C).

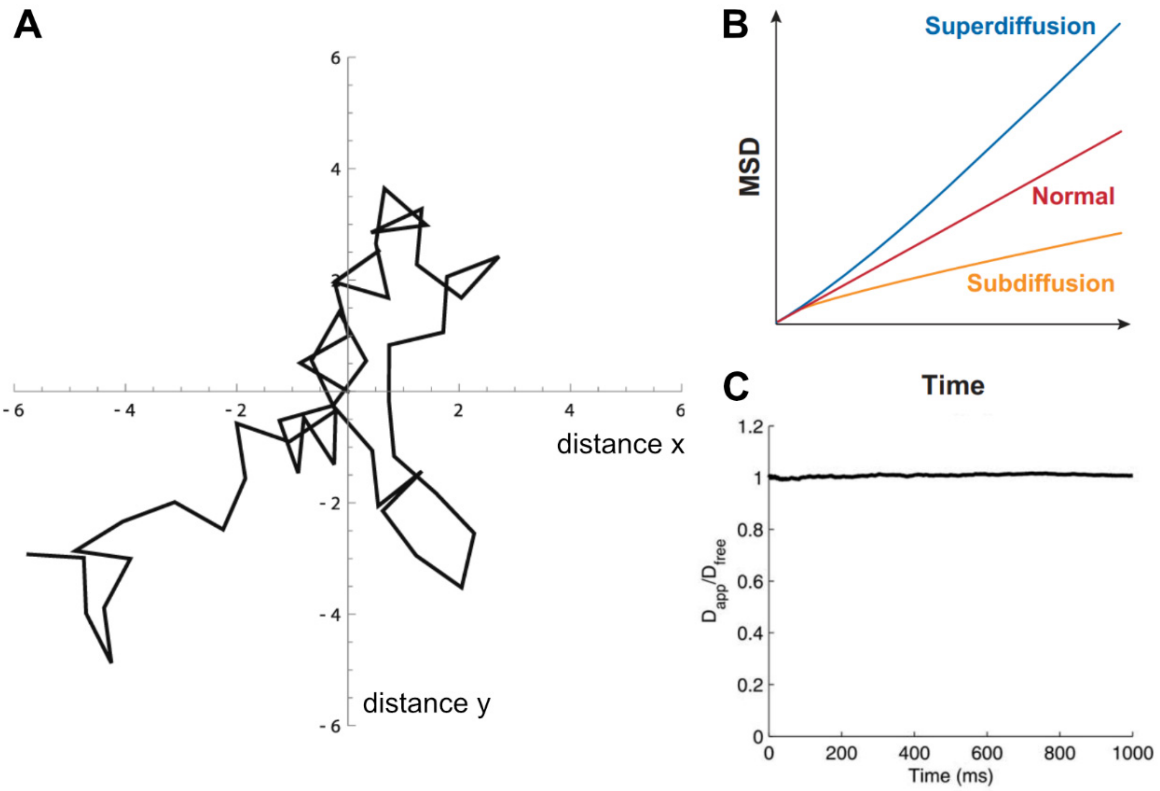

Figure 8: Dynamics of particle movement over time. A: Graph, displaying the trajectory of a particle in two dimensions (x and y) over time starting at point x=0; y=0. The position of the particle was determined in consistent time intervals. Modified from (Ma et al., 2021). **B:** Plot showing the change in mean square displacement (MSD) over time in cases of normal diffusion (red), superdiffusion (blue) and subdiffusion (yellow). Note that whilst the MSD changes linearly over time in the case of normal diffusion, it deviates in the cases of anomalous diffusion. Taken from (Dix and Verkman, 2008) C: Plot showing the change of the apparent diffusion coefficient (D_{App}) over time, in the case of normal diffusion. Note that D stays constant over time, which is characteristic for normal diffusion. Modified from (Santamaria et al., 2006).

Throughout the last decades, an increasing number of biological processes have been identified, which could not be explained by normal diffusion. These processes characteristically diverge from the predictions made for normal diffusion, either by long retention times between steps, or exceedingly fast jumps. The phenomena are termed subdiffusion and superdiffusion respectively (Klafter and Sokolov, 2005; Dix and Verkman, 2008) and are both types of

anomalous diffusion (Fig. 8 B). Whereas normal diffusion is characterized by a mean square displacement (MSD) which grows proportional to $D\tau$over time, neither super-, nor subdiffusion do so, with superdiffusion showing faster and subdiffusion showing lower changes in MSD (MacKintosh, 2012). Thus, *D* is not constant, but changes over time. Superdiffusion has been used describe animal behaviour including as the flight pattern of Albatrosses (Edwards et al., 2007). On the other hand, subdiffusion has been used to describe the diffusion of proteins across cell membranes (Kusumi et al., 1993; Ritchie et al., 2005) and in cellular environments (Banks and Fradin, 2005). As only subdiffusion is observed for biological processes, it is often referred to as anomalous diffusion (Santamaria et al., 2006, 2011). This work will therefore also use the term anomalous diffusion, to allude to subdiffusional characteristics.

Taken together diffusion describes the random movement of particles along a concentration gradient. In the cell, such particles include large proteins, even transporters, but also small, unbuffered molecules, including ions such as Na^+. Processes such as trapping influence the propagation of molecules, leading to anomalous diffusion. As diffusion is essential for the maintenance of intracellular concentrations and the shaping of transient signals, it has to be accounted to understand the fast-molecular processes, which occur in dendrites and other subcellular structures.

3.2 Physiological properties of dendritic diffusion

To understand the dynamics of Na^+ diffusion in the dendrite, one must consider the inter-dendritic properties, which could affect diffusional dynamics within the cytoplasm. There is extensive research which has been committed to the understanding of compound movement through the dendrite (Popov and Poo, 1992; Santamaria et al., 2006, 2011). Most of them report a slowing of compound diffusion throughout the dendrite over time which points to altered diffusion dynamics. This has been attributed to a number of characteristics including crowding of the dendrite, membrane charges and especially the density of spines seaming the dendrite.

The effects of dendritic crowding have been extensively studied, with a particular focus on diffusional dynamics in the dendrite. As such, the occurrence of intracellular crowding of proteins and organelles as well as the cytoskeleton have been shown to have an effect on intracellular dynamics, resulting in a severe reduction of the diffusion coefficient (Weiss et al., 2004; Dauty and Verkman, 2005). This has been shown to occur in studies which monitoring green fluorescent protein (GFP) movement throughout the cytoplasm (Baum et al., 2014; Di Rienzo et al., 2015). Furthermore, Ca^{2+} and dextran diffusion are also affected by intracellular organelles, leading to a 20-fold reduction of the diffusion coefficient (Biess et al., 2011). The

occurrence of proteins and organelles is extremely relevant for Ca^{2+} propagation, as the ion is buffered, limiting its movement to only a few µm from the point of intrusion.

Further studies suggest that the membrane charge contributes to the diffusional characteristics in the dendrite, as negative charge of the membrane and the cytoskeleton may influence the propagation of charged ions such as Na^+ (Qian and Sejnowski, 1989). On the other hand, the cable theory postulates that molecules move freely throughout the dendrite, without influence from intracellular organelles and membrane charges (Holcman and Yuste, 2015). It has been proposed that the cable model is good to use for electro-diffusion in structures which are larger than 1 µm (Qian and Sejnowski, 1989), such as giant squid axons or thick dendrites. However, membrane charges have to be considered in smaller structures such as spines or thin dendrites due to the small volume and thus close proximity to the charged membrane (Holcman and Yuste, 2015).

Previous work has also provided evidence, that anomalous diffusion is prevalent in spiny dendrites (Santamaria et al., 2006) (Fig. 9 A). Such work includes the tracking of uncaged fluorophores throughout spiny and smooth dendrites, and the generation of intensity profiles at specific timepoints. The convolution of such profile over time using a Gaussian fit allowed for the calculation of the variance ($<x^2>$) which can be identified as the MSD (Santamaria et al., 2006, 2011; Di Rienzo et al., 2015; Mohapatra et al., 2016) (Fig. 9 B). This analysis showed that movement of the fluorophore through spiny dendrites displays anomalous characteristics, which was not as severe in smooth dendrites. Therefore, determined diffusion coefficients did not stay constant, but decayed over time (Fig. 9 C). Further simulations showed that the degree of anomalous diffusion is dependent on the dendritic spine density. This led to the conclusion that molecules experience a process of trapping within spines, resulting in a slowing of lateral diffusion. Such an impact of morphological structures on lateral diffusion has also been proposed by comb-like models (Méndez and Iomin, 2013). Simulation studies of Cl^- movement, which is not buffered in the cytoplasm, imply spine density-dependent anomalous diffusion resulting in severely reduced D_{Cl^-} (Mohapatra et al., 2016). As Na^+ also diffuses freely throughout the cytoplasm, it is conceivable that spine densities of the dendrite also heavily influence its movement.

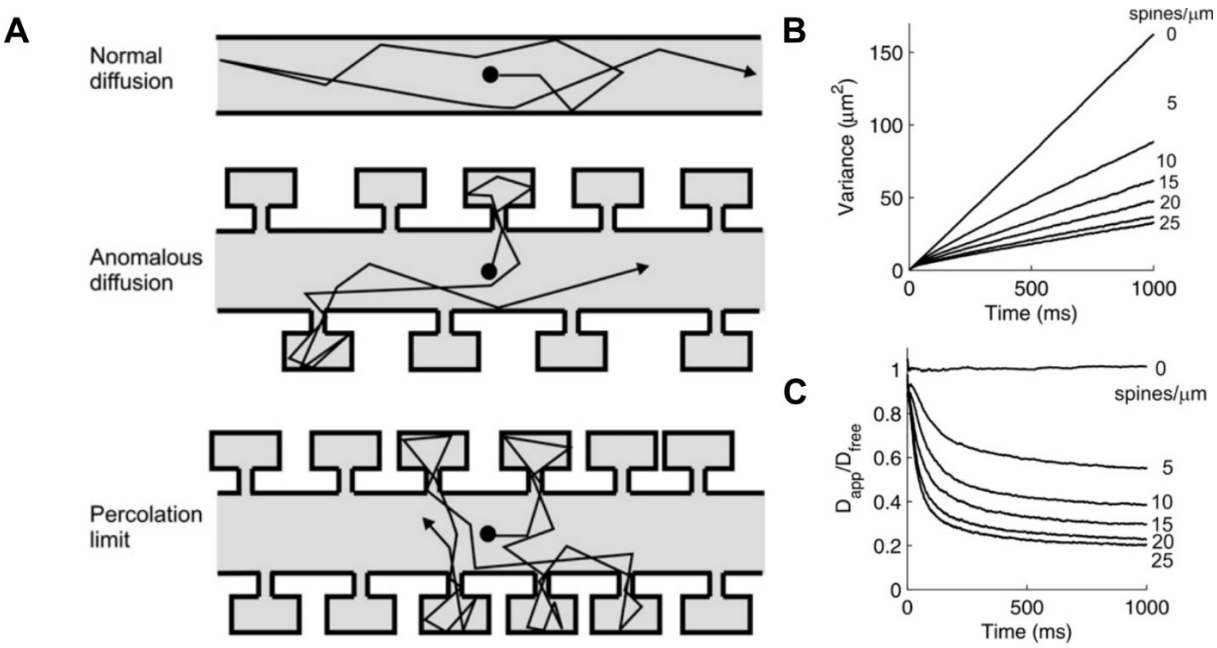

Figure 9: Anomalous diffusion in spiny dendrites. A: Schematic image showing the diffusion of compounds through a non-spiny dendrite (top) and dendrites with high (middle) and extremely high spine numbers (bottom), highlighting the compound movement throughout the dendrite (arrows). Note that the compound moves into the spine head, which ensues anomalous diffusion. **B:** Change of the spatial variance in both the smooth and spiny dendrites over time. Variance increased linearly in dendrites which exhibited 0 spines/µm. Increased spine numbers, led to a deviation from the trajectory. C: The resulting diffusion coefficients (D_{App}), calculated for the varying spine densities. Spineless dendrites did not show a change in (D_{App}) over time, indicating the occurrence of normal diffusion. Increased spine numbers led to a drastic reduction in (D_{App}), a clear indication of anomalous diffusion. Taken from (Santamaria et al., 2006).

Taken together a vast array of dendrite characteristics have been proposed to alter the diffusion of compounds and ions. These range from intracellular organelles and membrane charges to the dendrite's spine density. These characteristics have been shown to alter the diffusion of molecules which diffuse freely throughout the cytoplasm. This also includes Ions, such as Cl^-. Due to the importance of Na^+, its dynamics within the dendrite are of utmost importance, this includes its ability to diffuse through the dendrite laterally.

3.3 Ion diffusion in the dendrite

The spread of ions within the cytoplasm is affected by their molecular properties and is strongly dependent on whether the ion is buffered or moves more freely. Multiple studies have shown that Ca^{2+} is buffered upon entering the cell (Verkhratsky, 2002; Biess et al., 2011). Thus, Ca^{2+} diffusion through the dendrite from the point of intrusion is highly restricted and confined to microdomains (Korkotian et al., 2004; Korkotian and Segal, 2006; Santamaria et al., 2006; Biess et al., 2011) (Fig. 10 A). Na^+ on the other hand has been shown to move unbuffered throughout the cytoplasm and is thus able to spread through large segments of the axon or

dendrite (Fig. 10 B) (Fleidervish et al., 2010; Miyazaki and Ross, 2017). Furthermore, experiments which examine the dynamics of Na^+ and Ca^{2+}, in spiny dendrites report that whilst Ca^{2+} is confined in the spine head after synaptic stimulation, Na^+ manages to move out of the spine head and diffuses throughout the dendrite (Petrozzino et al., 1995; Miyazaki and Ross, 2017). Such studies highlight the importance of diffusional properties for the dynamics of Na^+ in subcellular structures, including neuronal axons and dendrites.

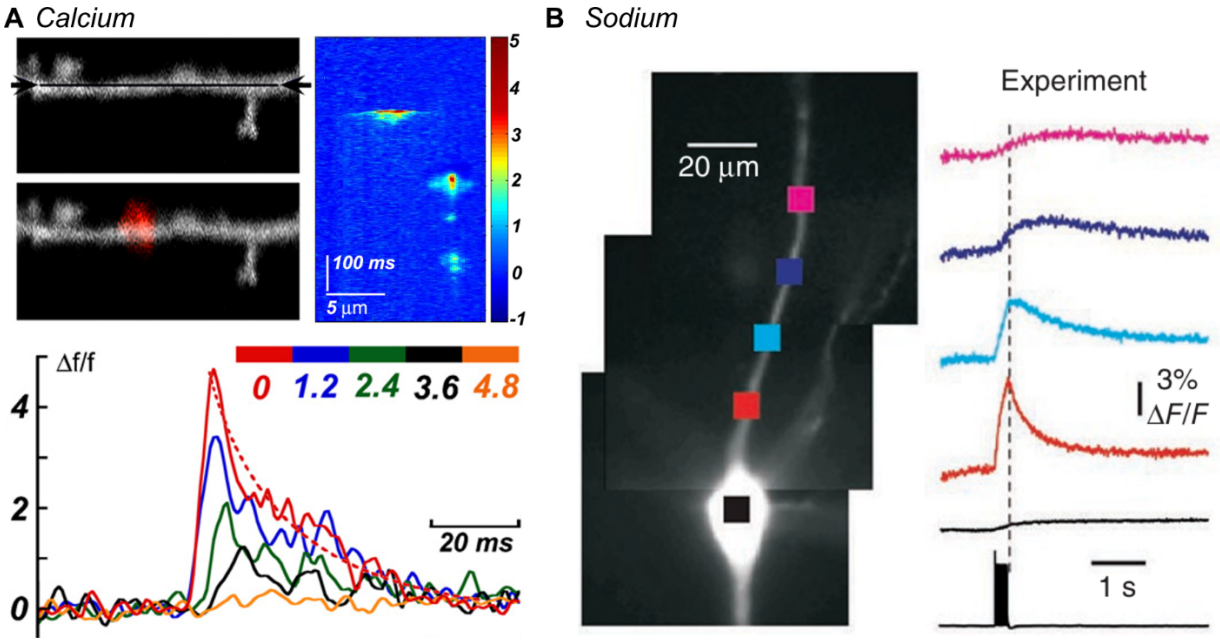

Figure 10: Dynamics of Na^+ and Ca^{2+} in subcellular structures. A: Measurement of flash photolyzed calcium dynamics in a spiny dendrite. Upper left: Images of the dendrite, which the linescan was performed on, as well as the regions which was photolyzed. Upper left: Image of the linescan, illustrating the change in $[Ca^{2+}]_i$ following the flash. Bottom: $[Ca^{2+}]_i$ transients, taken the linescan above with 0 representing the flash center. Transients are also shown for segments at a distance from 1.2,2.4,3.6 and 4.8 µm. Note that $[Ca^{2+}]_i$ were observable at a distance of > 4.8 µm. Taken from (Korkotian and Segal, 2006). B: $[Na^+]_i$ transients after a train of 10 Action potentials. Left: Image of a SBFI filled pyramidal neuron including its axon. Coloured boxes indicate the measured regions. Right: $[Na^+]_i$ transients measured at the indicated regions of interest after eliciting 10 action potentials. Note, that $[Na^+]_i$ transients were measurable at a distance of >60 µm from the soma, pointing to diffusion of Na^+ through the axon. Taken from (Fleidervish et al., 2010)

Due to the importance of Na^+ for the cell, its dynamics have been investigated in multiple systems over the last decades. Thus, diffusion coefficients of Na^+ have been determined in aqueous solution (~1500 $\mu m^2 \cdot s^{-1}$, (Lobo, 1993)) as well as in the cytosol of oocytes (790 $\mu m^2 \cdot s^{-1}$; (Albritton 1992)), lizard axons (1300 $\mu m^2 \cdot s^{-1}$; (David et al., 1997)) and muscle cells (600 $\mu m^2 \cdot s^{-1}$; (Kushmerick and Podolsky, 1969)). Further studies, which simulate Na^+ dynamics in subcellular structures like the axon and dendrite almost exclusively assume fast diffusion coefficients of 600 $\mu m^2 \cdot s^{-1}$ (Fleidervish et al., 2010; Miyazaki and Ross, 2017; Filipis and Canepari, 2021). However, little work has been done to experimentally establish the diffusion of Na^+ in the dendrite, the part of the cell most associated with frequent local increases of Na^+.

As previously described in 3.2, a number of publications suggest that diffusion of molecules and free diffusion ions, such as Cl^-, is altered, leading to a reduction in diffusional dynamics. Furthermore, rough estimation of the diffusion coefficient in primary dendrites report an apparent D_{Na+} of 330 $\mu m^2 \cdot s^{-1}$ in primary dendrites (Mondragão et al., 2016) indicating potential dampening of diffusional dynamics. However, such studies do not consider Na^+ diffusional dynamics over time and thus do not investigate the occurrence of normal or anomalous diffusion. Furthermore, these studies fail to assess the morphological properties of dendrites, which as described in 3.2 is reported to have an effect on lateral diffusion.

Thus, although Na^+ diffusion has been a matter of interest throughout the previous decades, work which has focused on the exact characteristics of Na^+ diffusion in dendrites have not been sufficiently conducted up to this point. Such measurements are very difficult to obtain with sufficient resolution due to the imaging frequency of needed for such fast processes and the structure of the dendrite. Previous work has been conducted using widefield imaging to achieve the frequency needed for the fast-diffusional dynamics of Na^+ (David et al., 1997; Fleidervish et al., 2010; Miyazaki and Ross, 2017). However, widefield imaging has difficulties resolving structures in deep tissue samples due to limited resolution in the z axis. For the evaluation of the diffusional characteristics, techniques which enable the evaluation of the morphology of the dendrites and offer a sufficient imaging frequency must be considered. Also, only the determination of the diffusion coefficient over time enables the investigation of diffusion characteristics, revealing the occurrence of normal or anomalous diffusion in dendrites. Such an analysis has not yet been undertaken for Na^+ movement in dendrites, but is of great importance if we are to understand dendritic ion dynamics. This is especially relevant for spiny dendrites, as repots suggest that spine densities alter diffusional characteristics.

4. The properties of dendritic spines and spine - dendrite coupling

Characteristically, dendrites of pyramidal neurons are seamed with spines, which function as postsynaptic site within the tripartite synapse. The crossing of molecules from spines into dendrites and back has been disputed over the last decades, with much work suggesting compartmentation of the spine from the dendrite. Moreover, it has been shown that such compartmentation is dependent on the spine's morphological attributes.

4.1 Spine morphology

It has been shown, that spines seam dendrites of pyramidal cells (Fig. 11 A) with a reported density of 6 to 22 spines per 10 µm (Harris and Stevens, 1989; Kirov et al., 1999; Konur et al., 2003; Ultanir et al., 2007; Niu et al., 2008; Perez-Cruz et al., 2011; Chapleau et al., 2012). The spine density is dependent on the dendrite order, with proximal broad dendrite

generally showing low spine numbers, while distal dendrites having high spine numbers. During development, morphological changes of the dendrite ensue an increasing number of spines and a change of spine morphology in a process termed synaptogenesis. The increase in spine numbers has been observed in multiple studies (Harris et al., 1992; Collin et al., 1997; Megıas et al., 2001; De Simoni et al., 2003; Ultanir et al., 2007). NMDAR have been described as a key factor for the increase in spine density during development, as NMDAR knockout mice showed significantly decreased spine numbers when compared to wild types (Ultanir et al., 2007).

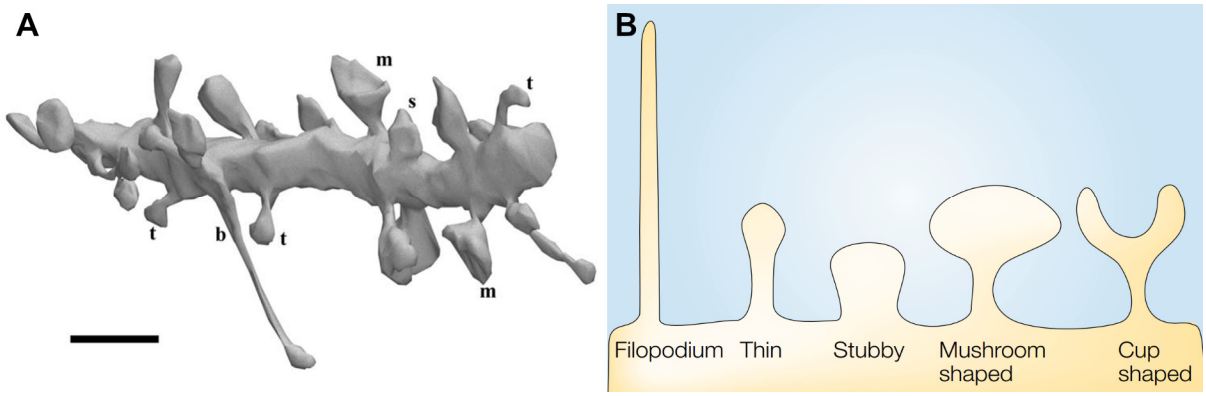

Figure 11: The morphology of spiny dendrites. A: Reconstructed electron microscopic image of a spiny dendrite with stubby (s), thin (t), and mushroom (m) and branched (b) spines. The scale represents 1 µm. Taken from (Fiala and Harris, 1999) **B:** Schematic representation of spines with different morphology, including filopodia, thin, stubby, mushroom and cup-shaped spines. Taken from (Hering and Sheng, 2001).

Morphologically spines are comprised of a spine head and a spine neck which connects to the dendrite. The spine head carries the PSD which includes anchor proteins and glutamate receptors, such as AMPAR and NMDAR. Spines are generally classified based on their morphology. As such spines are grouped in filopodia, stubby, thin, mushroom-shaped and cup-shaped (Peters and Kaiserman-Abramof, 1970; Son et al., 2011) (Fig. 11 B). Rarely, spines display a branched morphology (Fiala and Harris, 1999). However, work which has focused on such classifications has also often reported spines which were not suitable for such a defined classification. These were proposed to display intermediate morphologies between groups (Spaceck and Hartmann 1983; Peters and Kaiserman-Abramof, 1970; Harris et al., 1992; Harris and Kater, 1994; Arellano et al., 2007). This diversity of morphology and the limitations of optical resolution have raised the question of whether a defined classification of spines is suitable (Nägerl et al., 2008; Tønnesen et al., 2014).

The heterogeneity of spine morphology points to the ever-changing characteristic of the spine. Such a change in shape occurs during development and in matured spines, pointing to a high degree of plasticity.

4.2 Spine compartmentation

The compartmentation of the spine has been suggested and has been debated. It has been shown to be highly relevant, as it implies that synaptic strength of single spines is regulated independently, rendering spines as computational subunits of the neuron (Yuste and Denk, 1995; Shepherd, 1996; Matsuzaki et al., 2004). Throughout the last decades, studies have identified spines as being compartmentalized electrically ((Araya et al., 2007; Yuste, 2013; Araya et al., 2014) and biochemically (Yuste and Denk, 1995; Biess et al., 2007; Biess et al., 2011)). Biochemical compartmentation results in hindered diffusional coupling between spines and the dendrite (Svoboda et al., 1996; Biess et al., 2007). Notably, experiments concentrating on the conductance of ions indicate that whilst Ca^{2+} is primarily kept in the spine head, Na^{+} is able to pass from the spine head into the dendrite (Miyazaki and Ross, 2017), showing that compartmentation differs between ions.

Studies have also shown that the degree of compartmentation is highly heterogeneous and shaped by neuronal activity (Bloodgood and Sabatini, 2005). Experiments which focus on spine compartmentation include the measurement of Ca^{2+} dynamics from spine to dendrite after synaptic input, and fluorescence recovery after photobleaching (FRAP) experiments of fluorescent dyes (Tønnesen et al., 2014). This shows that spines have varying degrees of compartmentation from the dendrite with some spines showing complete electrical and diffusional isolation from the dendrite (Bloodgood and Sabatini, 2005; Yuste, 2013) (Fig. 12 A). Numerous publications attribute the degree of compartmentation to the morphology of the spine neck (Svoboda et al., 1996; Noguchi et al., 2005; Holcman and Schuss, 2011; Tønnesen et al., 2014). Notably, such work showed that the spine neck functions as an electrical (Araya et al., 2006; Araya et al., 2014; Jayant et al., 2017) and biochemical resistance (Svoboda et al 1996). Simulations which focus on the dynamics of the Calcium- calmodulin (CaM)- dependent protein kinase II (CaMKII) underline these effects, showing that stubby spines show a fast decrease of CaMKII in the spine head, whilst thin necked spines showed prolonged time constants (Byrne et al., 2011) (Fig. 12 B). Work which focused on the trajectory of compound diffusion in the spine suggest, that molecules which enter the spine head, experience trapping, and are thus limited in their ability to protrude to the dendrite (Fig. 12 C). The degree of trapping is thereby dependent on the morphology of the spine neck and the ability of the molecule to diffuse through the spine head (Biess et al., 2007). As such, spines with a long and narrow neck were compartmentalized to a stronger extent, than spines with short and broader necks. This also led to the conclusion, that the spines geometry defines its influence on the overall signaling within the dendrite (Takasaki and Sabatini, 2014; Tønnesen and Nägerl, 2016), with

spines displaying shorter and broader necks contributing more to the overall dendritic signaling.

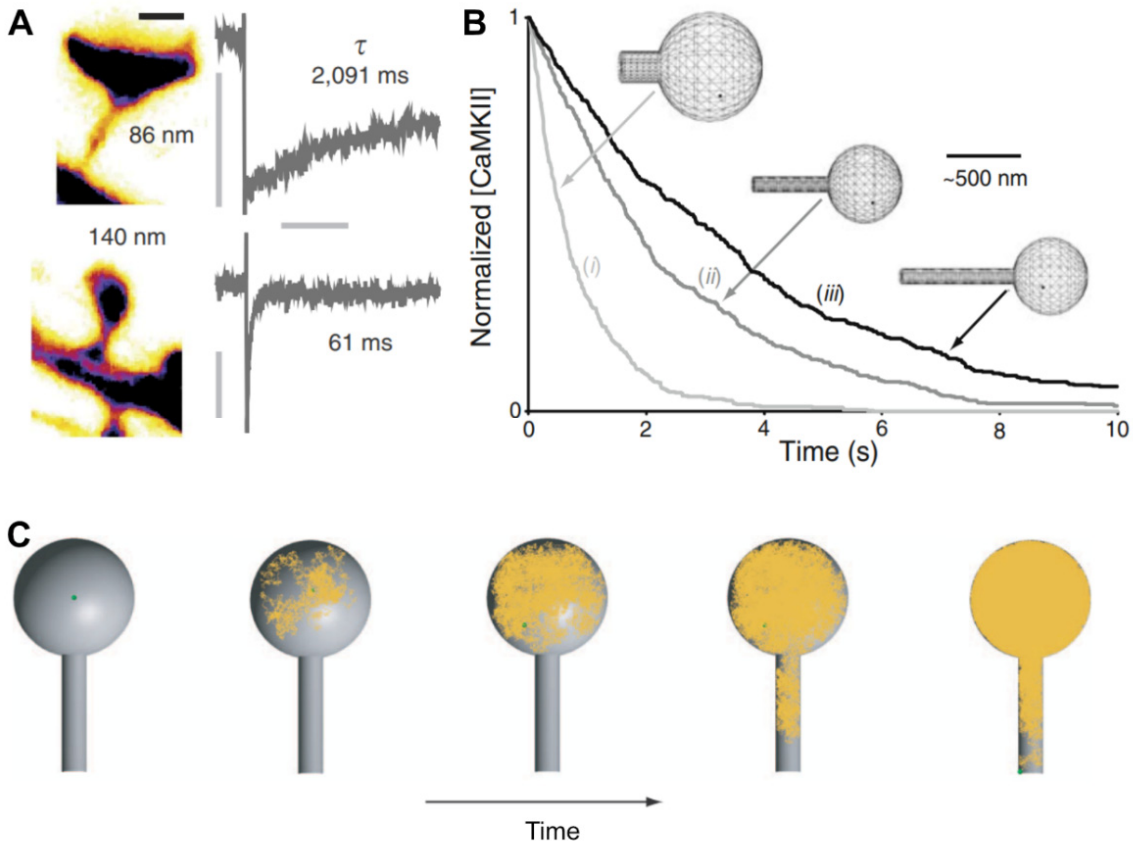

Figure 12: Compartmentation of spines. A: Visualization of fluorescence recovery after photobleaching (FRAP) experiments which were conducted in spines with thin (top) and thick (bottom) necks. Fluorescence recovery was severely prolonged in thin-necked spines, as compared to thick necked spines. Taken from (Tønnesen et al., 2014). **B:** Representations of trapping of CaMKII in spines of different morphology. Spines with a smaller head and neck need more time to recover from CaMKII increases, than spines with a thick neck and large head, indicating a stronger degree of trapping. Taken from (Byrne et al., 2011). **C:** Modelling of particle (blue dot) diffusion (yellow lines) within the spine. Notice that the particle diffuses throughout the entire spine before protruding back through the spine head, indicating a trapping of the particle. Taken from (Biess et al., 2007).

The morphology of the individual spine is influenced by the activation of glutamate receptors within the PSD which lead to a reshaping of cytoskeletal structure and thereby of the spine (Ackermann and Matus, 2003; Jourdain et al., 2003). Previous work has thereby shown an increase in spine head volume and a shortening and broadening of the spine neck upon repetitive stimulation (Segal and Andersen, 2000; Tønnesen et al., 2014) (Fig. 13). This results in a reduction of electrical and biochemical resistance given by the spine neck, which increases an electrical and biochemical conductance from the spine head into the dendrite. Such change of spine morphology is a reaction to synaptic transmission and shows the degree of plasticity that a single spine is subjected to. The ever-changing nature of spines also shows their ability to constantly process incoming synaptic information. Therefore, the spine has been recognized as the smallest computational unit of the neuron.

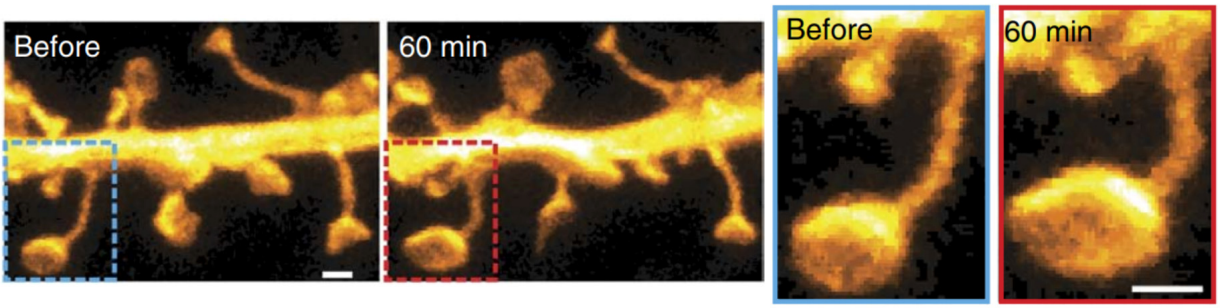

Figure 13: Change of spine morphology upon repetitive stimulation. Reconstructed stimulated emission depletion (STED) images of spiny dendrites before and after induction of repetitive stimulation for 60 min. Inserts show the individual spine which is highlighted on the left, emphasising an increase in head width and in neck width. Modified from (Tønnesen et al., 2014).

The prospect that molecules and ions such as Na^+ are able to cross into spine heads arouses the question on how dynamics are affected when entering the spine head through the dendrite. As especially Na^+ has a severe effect on the functioning of the cell, the trapping of Na^+ ions within neighboring spine heads would have great repercussions. However, studies, which focus on the diffusional coupling between spines and dendrites with regards to Na^+ are still lacking.

5. Aim of this study

Na^+ is recognized as excitatory charge carrier for the neuron and is coupled to various important transport processes. Its dynamics in the neuron are of great importance due to its effect on the cell during glutamatergic synaptic transmission. The clearance of Na^+ from the point of entry is crucial for the cell, as a prolonged increase in $[Na^+]_i$ leads to persistent depolarization and the breakdown of the Na^+ gradient. Previous work has shown that local $[Na^+]_i$ increases are predominantly cleared from the point of the entry via lateral diffusion. However, there is evidence showing that diffusional properties are altered in dendrites. Such an alteration of diffusional dynamics has been linked to the spine density of the dendrite. Due to its impact on the neuron, the determination of Na^+ diffusional dynamics in the dendrite is of utmost importance and yet largely unknown.

The aim of this doctoral thesis was to provide a study, which examines Na^+ diffusional dynamics in dendrites which are subjected to glutamatergic synaptic transmission and show morphological attributes which reportedly dampen lateral diffusion. To do so, the first aim of this study was to determine $[Na^+]_i$ in dendrites of CA1 pyramidal neurons and assess the influence of neuronal activity on dendritic $[Na^+]_i$. Secondly, this study investigated the diffusional spread of $[Na^+]_i$ along dendrites and into adjacent spines, thereby considering dendrite- spine coupling and examining possible spine compartmentation. Finally, this study examined the characteristics of lateral Na^+ diffusion along dendrites with different morphologies. It thereby considers the effect of increased spine densities, which reportedly lead to anomalous diffusion. As such, this study investigates whether such an altering of Na^+ diffusion takes place in dendrites.

To this end, fluorescent imaging of Na^+ specific dyes was used for the investigation of Na^+ dynamics in living CA1 pyramidal neurons in organotypic brain slices of the mouse. The use of fluorescent lifetime imaging (FLIM) thereby enabled measurements of absolute $[Na^+]_i$ in the dendritic tree. I also utilized local glutamate iontophoresis coupled with whole-cell patch clamp and two photon Na^+ imaging, to investigate the Na^+ spread throughout dendrites. This involved an experimental assessment of whether diffusion processes changed over time, which has never been conducted for Na^+ before. Three-dimensional reconstruction of the dendrite further enabled the correlation of diffusional characteristics to morphological attributes.

6. Technical background

6.1 Ion indicators as a mean to resolve intracellular ion changes

Understanding the ion dynamics in the brain on a cellular level has always been imperative for the comprehension of neuronal functioning. The use of ion sensitive fluorescent dyes has enabled the observation of intracellular ion changes in living cells (Harootunian et al., 1989; Donoso et al., 1992; Rose and Ransom, 1997). Whilst there are other techniques which can be used to determine ion fluxes into the cell, like the patch clamp technique (Sakmann and Neher, 1984), or the change of extracellular and intracellular ion concentrations through sharp tipped ion sensitive microelectrodes (Deitmer and Ellis, 1980; Haack et al., 2015), it is the imaging of ion sensitive fluorophores, which enabled the contemplation of ion changes within cellular networks down to dynamics in dendrites and spines (Minta and Tsien, 1989; Jaffe et al., 1992; Rose, 2012; Gerkau et al., 2019). Many fluorescent indicators have been established for various ions over the last decades, such as Oregon Green BAPTA-1 (OGB-1) (Ikegaya et al., 2005; Ziemens et al., 2019) and Fura-2 (Grynkiewicz et al., 1985) for the determination of Ca^{2+} dynamics, or BCECF for the observation of changes in pH (Everaerts et al., 2023). Na^+ sensors include Na^+-binding benzofuran isophosohthalate (SBFI;(Minta and Tsien, 1989)) and ION Natrium Green - 2 (ING-2) (Meyer et al., 2022) which change their fluorescence intensity upon the binding of Na^+. Both dyes have been used in a number of studies to show changes in Na^+ over time (Rose and Konnerth, 2001; Gerkau et al., 2017b; Gerkau et al., 2019; Pape and Rose, 2023).

SBFI and ING-2 have different spectral properties, as SBFI is excited by light in the UV range, whereas ING-2 is excited by blue light of around 525 nm in the visible light spectrum. Of the two, SBFI is a well-established tool for the detection of $[Na^+]_i$ transients not only in cell somata, but also in dendrites and astrocytic processes (Rose and Konnerth, 2001; Bennay et al., 2008; Langer et al., 2017; Gerkau et al., 2019). On the other hand, ING-2 not only changes its fluorescent intensity, but also its fluorescent lifetime upon the binding of Na^+ enabling fluorescent lifetime imaging (FLIM) (Meyer et al., 2022). The fluorescent lifetime is defined as the period, during which the fluorophore stays in an excited state, before returning to a ground state by emitting energy in form of fluorescence (Becker, 2015). A major benefit of FLIM is the ability to determine absolute ion concentrations within the cell and subcellular structures. This is in contrast to measuring changes in fluorescence intensity, which enables the observation of concertation changes over time with regard to the baseline. Therefore, in this work, the measurement of $[Na^+]_i$ in dendrites under resting conditions was done by FLIM of ING-2 filled neurons.

A drawback which FLIM faces, is the necessity to collect a sufficient number of photons, limiting the achievable temporal resolution of FLIM measurements. As such, FLIM often requires many tens of seconds (Zhang et al., 2020) which is why FLIM-based studies often suffer from poor temporal resolution or are only able to show static images (Roder and Hille, 2014; Rungta et al., 2015; Untiet et al., 2017; Meyer et al., 2019). As signaling in the brain occurs within milliseconds to seconds, such temporal resolution is insufficient for physiological measurements. Thus, imaging of fast Na^+ dynamics in dendrites and adjacent spines was conducted by measuring changes in fluorescence intensity of SBFI which is an established dye for the monitoring of Na^+ changes in such subcellular structures.

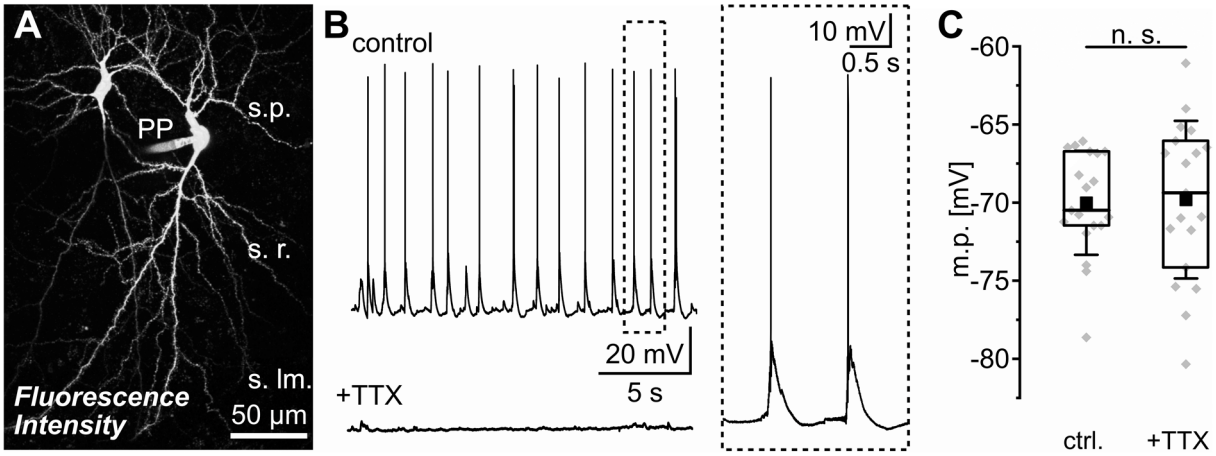

Figure 14: Whole cell patch clamp of a CA1 pyramidal neuron. **A:** Maximal projection of a CA1 neuron which was filled with SBFI via the patch pipette (PP). The cell was taken from a cultivated murine hippocampal slice and showed a basal and apical dendritic tree, protruding from the *stratum pyramidale* (s.p.) through the *stratum radiatum* (s. r.) and *stratum lacunosum moleculare* (s. lm.). **B:** Traces, showing exemplary current clamp measurements in control conditions and conditions containing 0.5 µM tetrodotoxin (TTX). In control conditions, cells showed a high frequency of action potential generation, which was silenced by TTX (bottom trace). **C:** Boxplot showing the baseline membrane potential in control conditions and in conditions containing TTX. Taken from (Nelson et al. in preparation).

The introduction of such dyes into the living cell is achievable in multiple ways. One possibility is to introduce the dye into the cell directly via whole cell patch clamp (Rose, 2003; Fleidervish et al., 2010; Rose, 2012; Gerkau et al., 2019) (Fig. 14 A). For this, a thin tipped pipette is brought into contact with the membrane of a targeted, single neuron. Rupturing of the cellular membrane underneath the pipette tip ensures a perforation of the cell with solution in the pipette, which also contains the desired ion indicator. Furthermore, the use of whole cell patch clamping enables the monitoring of the cell's electrophysiological properties (Fig. 14. B). This includes the measurement of the membrane potential and events such as action potentials (Fig. 14 B, C). It also permits the monitoring of currents, which are conducted over the membrane (Sakmann and Neher, 1984). In contrast to other methods, staining single neurons using whole cell patch clamp enables the consideration of subcellular structures, which has been essential for the analysis of morphological and ionic changes within dendrites and spines of pyramidal neurons. Filling the cell via whole-cell patch clamping has been performed on multiple occasions to resolve subcellular structures like axons or dendrites (De

Simoni et al., 2003) and is used in this work to introduce Na^+ indicators into CA1 pyramidal neurons.

Taken together, the use of fluorescent dyes enables the quantification of ion dynamics in the living tissue and has thus been used throughout the last decades. Na^+ indicator dyes SBFI and ING-2 have thereby been characterized to a great extent and have been used in multiple publications, to decipher the dynamics of Na^+ in brain tissue. The filling of fluorescent dyes into single cells via the whole cell patch clamp technique also allows the measurement of Na^+ dynamics in subcellular structures especially dendrites. Lastly, FLIM enables the determination of absolute ion concentrations in cells and subcellular structures compared to other previous used dyes and techniques. However, these measurements are temporally restricted, making it difficult to resolve the fast $[ion]_i$ dynamics. In this study, I used FLIM of ING-2 to determine baseline $[Na^+]_i$ within the apical dendritic tree. For the determination of dendritic $[Na^+]_i$ dynamics, I also performed imaging of SBFI fluorescence intensity in dendrites and spines. A dye which is well established for the monitoring of fast Na^+ dynamics in subcellular structures.

7. Results and discussion

7.1 The CA1 neuron in the organotypic slice resembles in vivo/in situ conditions

To establish $[Na^+]_i$ and Na^+ dynamics in the dendritic tree, in this work experiments were conducted on pyramidal CA1 neurons of the hippocampus. These are a well-established model for glutamatergic synaptic transmission and well known for the occurrence of spines upon dendrites within the dendritic tree. All experiments were conducted in organotypic hippocampal brain slice cultures (ORCs). These are brain tissue slices, which are cultivated ex vivo and contain all cell types of the brain, maintaining its 3-dimensional architecture. Organotypic brain slices have been used over many decades and have been well established for many different brain areas, such as cerebellum (Gähwiler, 1981), cortex (Giesing et al., 1975; Everaerts et al., 2023; Pape and Rose, 2023) and hippocampus (Stoppini et al., 1991; Buchs et al., 1993; De Simoni et al., 2003; Lerchundi et al., 2019), just to name a few.

Organotypic slices allow the cultivation of slices over long time periods, ranging from days up to several weeks and even months, compared to a survival of several hours with acute tissue slices. During this cultivation period, slices experience flattening. Such flattening is an important macroscopic sign that the slices are healthy (Humpel, 2015). The process of flattening also ensures that the elaborate structure of cells such as CA1 pyramidal neurons are contained within a confined 3-dimensional space (De Simoni et al., 2003). This is very beneficial for imaging experiments, as it allows the consideration of a large area within the

focal plane. This is of particular importance, as it enabled the consideration of long dendrite segments within one focal plane. Although flattening of the organotypic slice occurs, reports state that CA1 neurons maintain their general morphology (Gähwiler, 1984b, a, 1988; Stoppini et al., 1991). Filling single CA1 pyramidal neurons via whole-cell patch clamp confirms this observation, as cells do show the characteristic apical and basal dendrites which ramify into the dendritic tree (Fig. 14 A). In general, the apical dendritic tree often showed a high degree of ramification, which is in line with publications, stating a stronger arborization of CA1 neurons derived from organotypic slices, as opposed to neurons from acute slices (De Simoni et al., 2003). Pyramidal cells often showed a shortened primary dendrite, with first major ramifications in the *stratum radiatum*. Such morphology is in line with earlier reports, stating that CA1 pyramidal neurons show either long protrusion of one primary apical dendrite throughout the *stratum radiatum* and stratum *lacunosum moleculare*, or a direct ramification of the apical dendrite near the soma (Bannister and Larkman, 1995b, a). Such characteristics are also found in pyramidal cells on top cell layers of the subiculum (Harris et al., 2001). Previous work has suggested that the length of the primary dendrite varies according to the cell layer depth, with neurons at the superficial edge displaying shortened primary dendrites (Harris et al., 2001). The flattening of cultivated slices could therefore account for the tendency of neurons to display similar morphological characteristics.

Apical and basal dendrites of dye-filled pyramidal neurons were typically seamed with spines, which is characteristic for pyramidal neurons (Fig 15 A). This indicates that glutamatergic signaling and synaptic integrity is preserved. Further work developed at the Department of Biology and Biotechnology at the Ruhr University in Bochum and in which implementation I was involved, utilized the transgenetic glutamate indicator iGluSNFr, to show that glutamate is released by pyramidal cells within organotypic slices (Ziebarth, …, **Nelson**, et al., under review). This work shows that glutamate is released spontaneously at sites in the cortex. Such spontaneous glutamate transmission indicates neuronal activity and viability within the organotypic slice, as it also is reported to occur in vivo or in acute slice preparations (Xie 2016). Furthermore, patch clamp experiments, conducted on CA1 pyramidal neurons, revealed a high degree of neuronal activity and AP generation, which was dampened by selective inhibition of Na_v by 0.5 µM Tetrodotoxin (TTX) (Fig. 14 B, C). This is in line with previous work, reporting high neuronal activity of CA1 pyramidal cells in organotypic hippocampal slices (Müller et al., 1993; De Simoni et al., 2003) and shows that neuronal connectivity and activity is preserved in the slice (Gähwiler, 1988; Stoppini et al., 1991; Torp et al., 1992; Okamoto et al., 2014). These reports also show that cellular activity in organotypic slices represents is similar to activity levels measured *in vivo* (Okamoto et al., 2014).

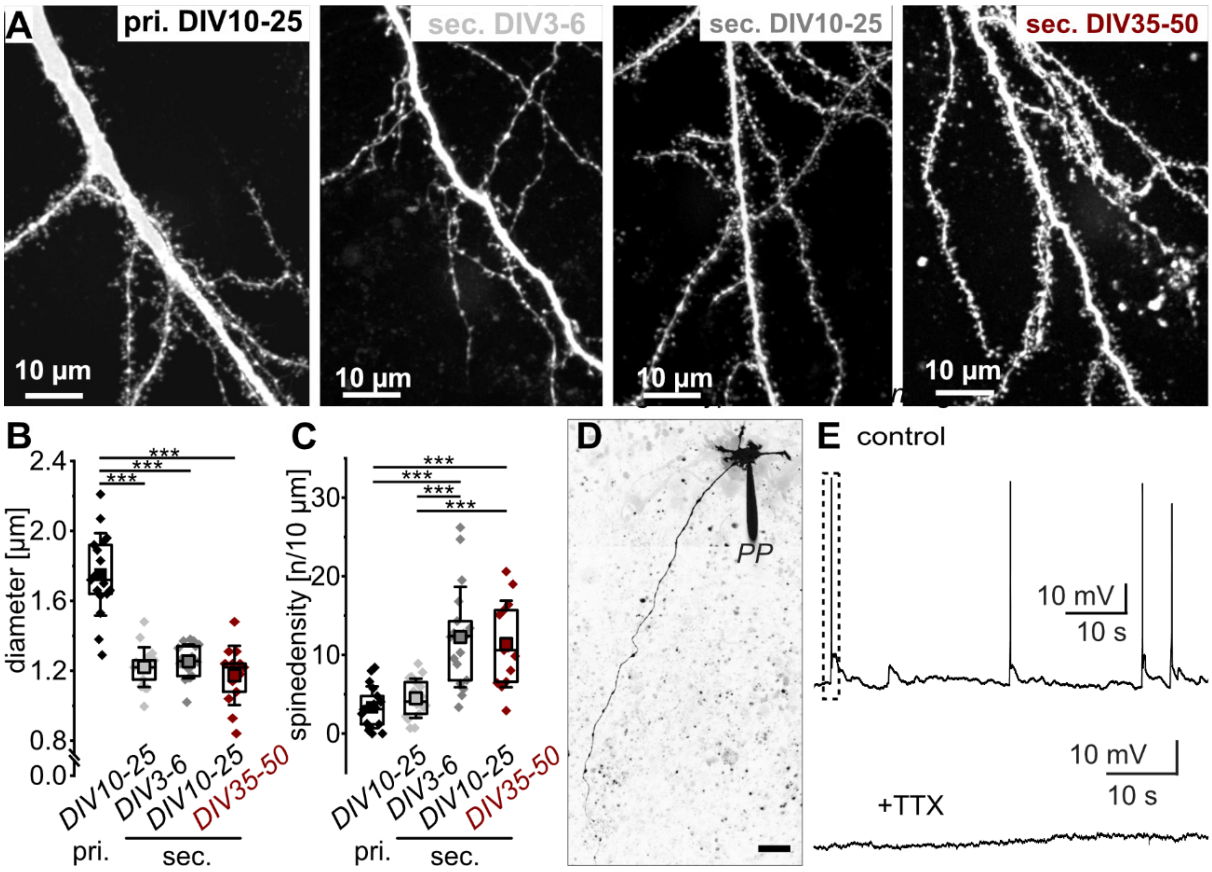

Figure 15: Characterization of neurons in organotypic slices of mouse brain and human brain organoids. A: Maximal projections of secondary dendrites filled with SBFI via whole cell patch clamp. The patched CA1 neurons were derived from young (DIV3-6) and old (DIV 35-54) organotypic slices of mouse brain. Note that z-stacks were subjected to deconvolution before generating the depicted maximal projections. **B, C:** Boxplots comparing the dendrite diameter and spine density in primary dendrites (DIV 10-25, black diamonds) and secondary dendrites which were subjected to different cultivation periods, incorporating DIV 3-6 (n=17; light grey diamond), DIV 10-25 (n=18, dark grey diamonds) and DIV 35-54 (n=13, red diamonds). **D**: Maximal projection of a neuron of an organotypic slice of a human brain organoid. Cells also displayed long dendrites, which protruded through the slice. **E**: traces showing spontaneously generated APs in human brain organoids-derived patched neurons, which were abolished in conditions containing TTX. A,B,C taken from Nelson et al. in preparation; D and E Modified from (Petersilie et al., 2024).

The degree of neuronal activity might lead to the generation of high synaptic densities and the generation of well-developed spines. Multiple publications suggest this to be the case, showing that dendrites of the CA1 pyramidal cells receive a dense glutamatergic input (Torp et al., 1992; Buchs et al., 1993; Müller et al., 1993). In general, previous work reports spine densities of about 6-10 spines per 10 µm in organotypic slice cultures derived from rats (Collin et al., 1997; Pozzo-Miller et al., 1999; De Simoni et al., 2003) and 10 spines per 10 µm in cultures derived from mice (Michaelsen-Preusse et al., 2014). Morphological analysis conducted in this project also leads to similar spine numbers with distal secondary dendrites displaying an average of 12 spines per 10 µm (Fig. 15 E). The use of organotypic slice cultures which were subjected to varying cultivation durations further showed that spine densities increased between 3-6 and 10-25 days of cultivation (days in vitro=DIV), but did not differ between 10-25 and 35-50 days in cultivation. This is very much in line with work, which

investigates the maturation of the dendrite and report increasing spine numbers until the third week of cultivation or age (Buchs et al., 1993; Ziv and Smith, 1996; Collin et al., 1997; De Simoni et al., 2003; Roelandse et al., 2003; Ultanir et al., 2007; Chapleau et al., 2012). Studies report, that during that glutamatergic synapses are preserved during the cultivation of slices, and that a high degree of plasticity within the dendrite and the spine takes place (Torp et al., 1992; Buchs et al., 1993; Bahr et al., 1994; Dailey and Smith, 1996; De Simoni et al., 2003; Nikonenko et al., 2013).

The benefits of organotypic slices, namely the preservation and strengthening of synaptic connections, the generation of spines and a neuronal activity which resembles in vivo measurements, have led to the establishment of ORCs from human brain organoids (Giandomenico et al., 2019; Giandomenico et al., 2021). As such, our cultivation technique has been used in combination with cortical slices from human brain organoids (Petersilie et al., 2024). In this project, I was able to perform whole cell patch clamp recordings of cells within the cultivated slice (Fig. 15 D, E). These cells displayed spontaneous activity and were able to generate AP, which were silenced upon TTX application (Fig. 15 E), therefore showing characteristics of mature neurons. Furthermore, imaging experiments could show that cells had spines seaming the dendrite, underlining the occurrence of mature pyramidal neurons.

Taken together, organotypic slices have been established as an excellent preparation for the investigation of neuronal processes, as synaptic cellular morphology, as well as synaptic connections, are preserved during the cultivation process. In addition, neurons derived from organotypic slices reportedly show a high degree of cellular activity. Also, the flattening of the slice enables the consideration of long dendritic segments within the focal plane, during experiments. Therefore, organotypic slices are not only suitable, but also preferable for work which utilizes fluorescent imaging in dendrites for the observation of ion dynamics, as it is performed in this study.

7.2 $[Na^+]_i$ baseline under resting conditions in the dendritic tree

As previously described in chapter 2, the dynamics of ions such as Na^+, are heavily dependent on the permeability for the given ion, as well as its specific intracellular and extracellular concentrations. Thus, the measurement of $[Na^+]_i$ is of extreme importance for the understanding of Na^+ dynamics during and following transient signals. Previous studies which coupled whole cell patch clamping to Na^+ imaging have successfully been used for the determination of $[Na^+]_i$ at the cell soma (Mondragão et al., 2016; Ziemens et al., 2019). However, such studies neglect possible differences in $[Na^+]_i$ in subcellular structures like dendrites and axons. As synaptic transmission and signaling take place within the dendritic tree, concentrations established in the soma may not reflect the concentrations in dendrites. In recent years, FLIM has proven itself as a method, which enables the non-invasive

determination of ion concentrations and has been used to measure the concentrations of Ca^{2+} and Cl^- in neurons and astrocytes (Zheng et al., 2015; Zheng et al., 2018; Weilinger et al., 2022), including their dendritic tree and astrocytic processes. Filling the cell with the Na^+-sensitive dye ING-2 enabled the determination $[Na^+]_i$ in primary and secondary dendrites (Fig. 16 A,B). As such, this work provides measurements of absolute $[Na^+]_i$ within the dendritic tree.

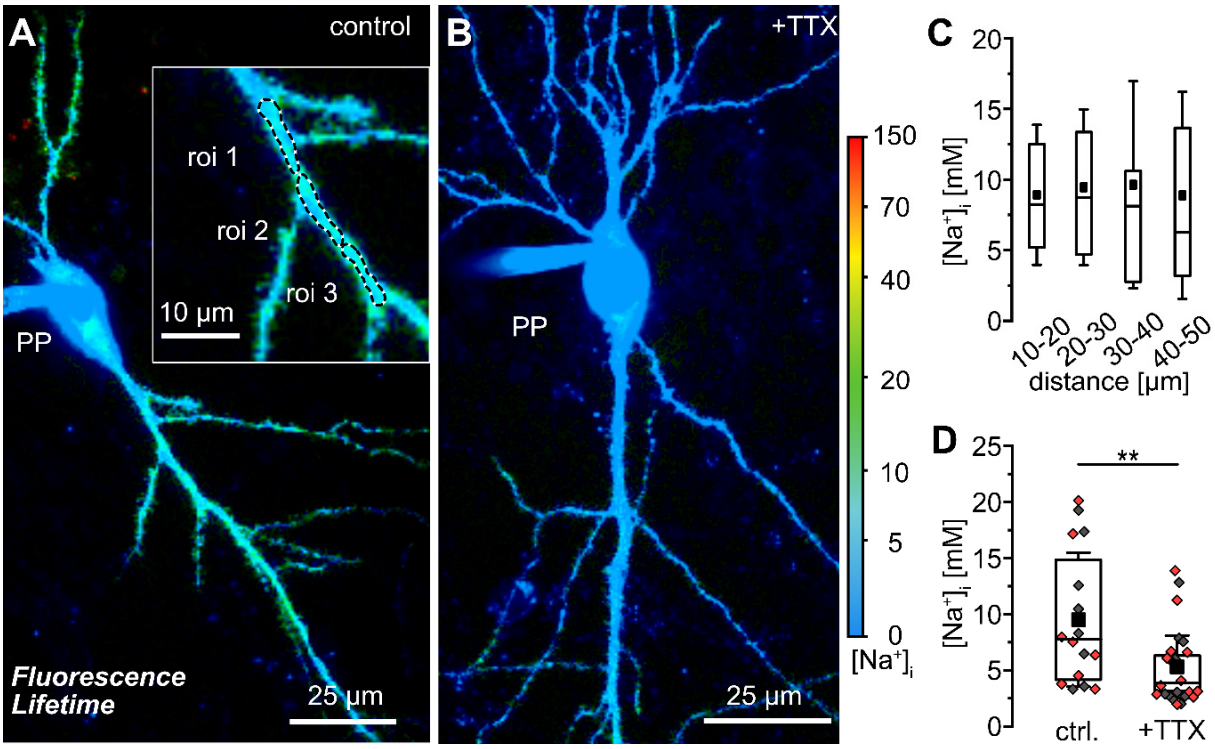

Figure 16: $[Na^+]_i$ in the dendritic tree of CA1 neurons. A: Maximal projection of a fast fluorescent lifetime image (fastFLIM) of a CA1 neuron filled with ING-2. **B:** Maximal projection of a CA1 neuron which was subjected to TTX. Note the change in coloration, which shows a decrease in $[Na^+]_i$ as indicated by the color code on the right. **C:** $[Na^+]_i$ throughout the primary dendrite at increasing distance from the soma in control conditions, which did not show any significant change. **D:** Boxplot showing $[Na^+]_i$ in primary (grey diamonds) and secondary (red diamonds) dendrites in control conditions and with TTX. Taken from (Nelson et al. in preparation).

The data showed dendritic $[Na^+]_i$ in the range of 9.5 mM (Fig. 16 D). This is well within expected values as multiple publications have reported concentrations of 9-11 mM in the soma of hippocampal neuronal cultures (Rose and Ransom, 1997; Diarra et al., 2001; Azarias et al., 2013) and 10-15 mM in the soma of pyramidal neurons from hippocampal and cortical acute slices (Pisani et al., 1998; Langer and Rose, 2009; Kelly and Rose, 2010; Karus et al., 2015; Mondragão et al., 2016; Meyer et al., 2022).

The data also showed that resting $[Na^+]_i$ did not change throughout the primary dendrite and between primary and secondary dendrites (Fig. 16 C,D) which is in line with work focusing on Cl^- and Ca^{2+} concentrations throughout the dendritic tree (Zheng et al., 2015; Zheng et al., 2018; Weilinger et al., 2022). In contrast to this, studies reported $[ion]_i$ changes depending on

the order of astrocytic processes which was not observable in neuronal dendrites (Zheng et al., 2015; Zheng et al., 2018; Weilinger et al., 2022).

To study the effects of spontaneous neuronal signaling on dendritic $[Na^+]_i$, slices were subjected to 0.5 µM TTX which led to a drop in dendritic $[Na^+]_i$ to 5.3 mM (Fig. 16 D). Such a TTX mediated drop in baseline $[Na^+]_i$ has not been reported in studies which focus on the soma (Rose and Ransom, 1997). However, dendrites are also heavily subjected to ion fluctuations caused by synaptic transmission and back propagating action potentials which lead to long lasting $[Na^+]_i$ transients (Rose et al., 1999; Lamy and Chatton, 2011; Gerkau et al., 2019). It is therefore probable that the silencing of such events through TTX results in a drop in dendritic $[Na^+]_i$. as has been shown in this study. Furthermore, the data presented in this study emphasize the need for a better understanding of ion dynamics within the dendritic tree as data taken from the soma do not aptly reflect the processes, that occur on a dendritic level.

Taken together, the data shows that FLIM measurements using the Na^+ indicator ING-2 enabled the observation of $[Na^+]_i$ within the dendritic tree. $[Na^+]_i$ is thereby homogeneously distributed throughout the dendritic tree. Furthermore, the TTX mediated silencing of neuronal activity leads to an significant reduction of $[Na^+]_i$ which has not been observed in previous publications which focus on neuronal stomata. The data presented in this study thus shows that dendritic $[Na^+]_i$ is influenced by neuronal activity. This highlights the need for an understanding of the processes which regulate $[Na^+]_i$ in the dendrite during synaptic transmission. As local $[Na^+]_i$ increases are reportedly cleared by lateral diffusion, the understanding of the diffusional dynamics in the dendrite is of great importance.

7.3 Quantitative imaging of glutamate-evoked signaling using FLIM

As I was interested in Na^+ dynamics in the dendritic tree, I aspired to introduce a technique which enabled a local intrusion of Na^+ into the dendrite. For this, I utilized the iontophoresis of glutamate through a sharp micropipette (90-150 MΩ) onto the dendrite. A number of studies have performed similar experimental procedure, applying glutamate, GABA or NMDA, for the targeted stimulation of dendrites (Müller and Remy, 2013) and astrocytic processes (Ziemens et al., 2019).

Glutamate-induced changes in $[Na^+]_i$ were measured using FLIM of ING-2, which enabled the observation of baseline $[Na^+]_i$, as well as $[Na^+]_i$ elevations. As previously described in chapter 7.1, the necessity to collect a sufficient number of photons severely limits the temporal resolution of FLIM measurements. However, there is constant progress with regards to the obtainable imaging frequency, enabling imaging of $[Ca^{2+}]_i$ in living tissue, at frequency of multiple Hz (Zheng et al., 2015). In addition, experiments measuring $[Na^+]_i$ changes in ING-2 stained neurons in the *stratum pyramidale* were achieved at 0.5 Hz (Meyer et al., 2022). This work went even further achieving frame-based imaging with a temporal resolution of 5 Hz (10

Hz imaging frequency; binning of 2 frames) on dendrites of CA1 neurons, whilst performing glutamate iontophoresis (Fig. 17). The presented data show FLIM measurements of glutamate iontophoresis induced $[Na^+]_i$ transients within dendrites. The applied glutamate led to an expected local increase of $[Na^+]_i$. After reaching its peak, $[Na^+]_i$ returned to baseline monoexponentially. Previous work, which focused on $[Na^+]_i$ changes in the soma, showed an overall similar trajectory (Meyer et al., 2022). Furthermore, experiments which included the activation of synaptic release or exogenous application of glutamate, showed very comparable $[Na^+]_i$ transients, when monitoring changes in fluorescence intensity of Na^+ sensitive dyes (Lasser-Ross and Ross, 1992; Knöpfel et al., 2000; Rose and Konnerth, 2001; Meier et al., 2006; Bennay et al., 2008; Miyazaki and Ross, 2015; Gerkau et al., 2019; Miyazaki et al., 2019; Meyer et al., 2022). The use of whole cell patch clamp also enabled the monitoring of currents, which were measured at the soma. Glutamate iontophoresis led to a net influx (Fig. 17 B insert). The coinciding rise in $[Na^+]_i$ indicates, that the measured influxes can be attributed to Na^+ intrusion. This is in line with a number of publications which monitored fluxes during synaptic stimulation and direct application of glutamate in neurons and astrocytes (Bennay et al., 2008; Langer et al., 2017; Gerkau et al., 2019).

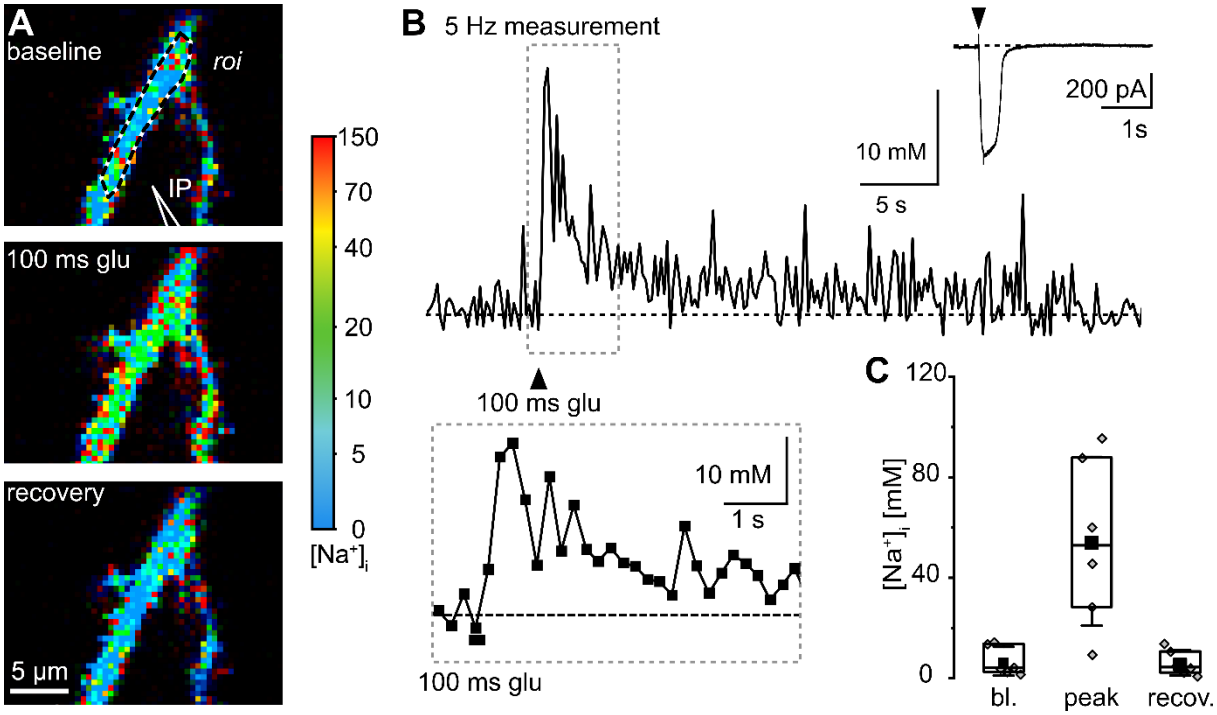

Figure 17: Change of dendritic $[Na^+]_i$ upon glutamate iontophoresis. A: Fluorescent lifetime images of an ING-2-filled dendrite, subjected to glutamate iontophoresis. Notice the change of coloration from blue to green and back to blue, indicating an increase in $[Na^+]_i$ during the application of glutamate via the iontophoresis pipette (IP). **B:** Traces taken from the experiment shown in A. Traces have a frequency of 5 Hz (10 Hz imaging frequency and 2-fold binning). The trace shows an increase in $[Na^+]_i$ upon glutamate iontophoresis. Insert shows the simultaneously measured influx, which was measured via the soma-based patch pipette. Zoom in beneath highlights the resolution of the signal. **C:** Boxplot, showing $[Na^+]_i$ at baseline, at the amplitudes peak and after recovering. Taken from (Nelson et al. in preparation).

The use of FLIM enabled the direct measurement of absolute $[Na^+]_i$. This also includes the determination of peak $[Na^+]_i$, as well as baseline $[Na^+]_i$ before glutamate stimulation. This contrasts measurement of fluorescence intensity, which enables the determination of $\Delta[Na^+]_i$ by measuring a change in fluorescence with regard to the baseline ($\Delta F/F_0$). Such measurements therefore give no information about the resting $[Na^+]_i$ of the individual cell or subcellular structure. The use of FLIM is therefore preferable, as it allows the consideration of resting $[Na^+]_i$ in individual cells and subcellular structures. Due to long photon acquisition which are necessary for FLIM, fast processes have not been resolvable in the past. The data presented in this study, however show the capability to resolve local glutamate induced $[Na^+]_i$. This was achieved as development of FLIM-based imaging techniques is pushing forward, enabling increased temporal resolution. Therefore, the data shows, that FLIM can be used in studies, which consider $[Na^+]_i$ dynamics on a timescale of multiple seconds. However, as $[Na^+]_i$ has a reported diffusion coefficient of 600-1300 $\mu m^2\ s^{-1}$ (Kushmerick and Podolsky, 1969; David et al., 1997) within the cell, the established imaging frequency of 5 Hz was not satisfactory for the investigation of dendritic Na^+ dynamics. To increase imaging frequency, needed for the evaluation of fast Na^+ dynamics, I performed linescanning of the Na^+ indicator SBFI, which enabled the resolution of multiple hundred Hz.

7.4 Fast dynamic imaging of Na^+ through the use of linescans

In order to resolve the extremely fast dynamics which occur in subcellular structures, multiple imaging techniques have been introduced. A common method is based on widefield imaging with cameras, which enable an imaging frequency of around 100 Hz (Santamaria et al., 2006; Fleidervish et al., 2010; Miyazaki and Ross, 2017). A drawback when using widefield imaging is the insufficient resolution in deep tissue preparations also preventing a satisfactory representation of the dendrite's morphology (Mancuso et al., 2013). The use of two photon imaging on the other hand, as was performed in this study, enables the satisfactory resolution of cellular structures in living tissue, but is severely limited in its temporal resolution, when scanning the entire field of view.

In order to achieve the necessary imaging frequency of >200 Hz with the two-photon microscope, I performed linescans on dendrites which were filled with the Na^+ sensitive dye SBFI via a patch pipette (Fig. 18 A). During measurements, a single line, rather than a whole frame, is chosen and scanned by the laser. The rate of acquisition is thereby determined by the length of the chosen line and the pixel dwell time. As such, linescanning enabled an imaging frequency of multiple hundred Hz (200 - 700 Hz) suitable for the quantification of fast Na^+ dynamics (Fig 18). Due to its benefits, linescanning has been used in a vast number of publications, focusing on various scientific questions such as the volume changes of brain

capillaries (Coelho-Santos et al., 2021) and overall ion dynamics in dendrites and spines (Rose et al., 1999; Goldberg et al., 2003; Korkotian et al., 2004; Korkotian and Segal, 2006).

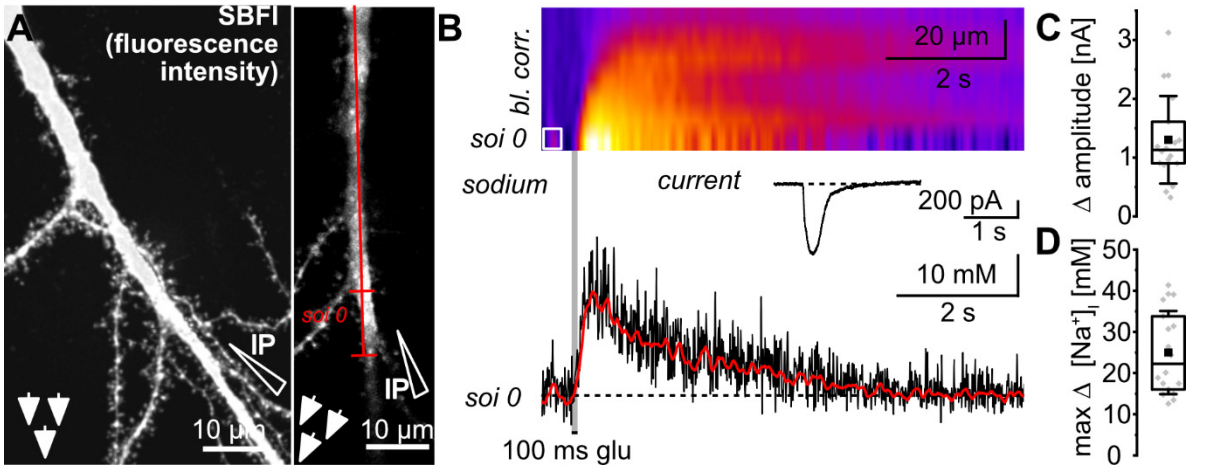

Figure 18: Linescanning of glutamate-evoked $[Na^+]_i$ signals. A: Maximal projection of a primary dendrite, filled with the Na^+ indicator dye SBFI. The image includes a visualization of the iontophoresis pipette (IP), which was used to administer glutamate. Perfusion direction is indicated by three arrows. Right, image of the dendrite in the plane, which was used to conduct the measurement. The red line indicates the trajectory of the performed linescan, with the portrayed segment of interest (soi). **B**: Baseline corrected image of the linescan over time, as provided by the python-based customized program. $[Na^+]_i$ transient measured at the soi closest to the iontophoresis pipette (soi0), as given by the python-based program after baseline correction (black) and after filtering (red). Insert depicts the simultaneous current measured via the patch pipette**. C,D**: Box plots showing Δ current amplitude (n=18 N=18), measured at the soma via whole cell patch clamp and max $\Delta[Na^+]_i$ (n=18;N=18) as imaged in primary dendrites. Taken from (Nelson et al. in preparation).

The processes behind glutamate-mediated Na^+ intrusions have been studied in length throughout the past years, identifying ionotropic glutamate receptors as key factors for Na^+ intrusion (Watt et al., 2000; Rose and Konnerth, 2001; Miyazaki and Ross, 2017). The first step in determining the dynamics of Na^+ movement throughout the dendrite was to verify the key factors for Na^+ influx. Blocking of the key ionotropic receptors AMPAR and NMDAR with the antagonists CNQX and AP5 led to a strong decrease in both dendritic $[Na^+]_i$ signals, as well as currents measured at the soma via whole-cell patch clamp (Fig. 19). This proves that both ionotropic ion channels mediate Na^+ intrusion, which is very much in line with previous data (Rose and Konnerth, 2001; Ziemens et al., 2019). The data presented in this work also confirms data in previous publications, which showed the extent of Na^+ intrusion mediated through NMDAR and AMPAR though blocking of the receptors (Ziemens et al., 2019).

Taken together, the data presented in this work show that linescanning of SBFI filled dendrites enabled the imaging of fast dendritic $[Na^+]_i$ transients. The data also indicated that $[Na^+]_i$ signals were primarily induced by the activation of the glutamate receptors AMPAR and NMDAR which affirms, that Na^+ intrusion is strongly mediated through synaptic activity and the resulting glutamate transmission.

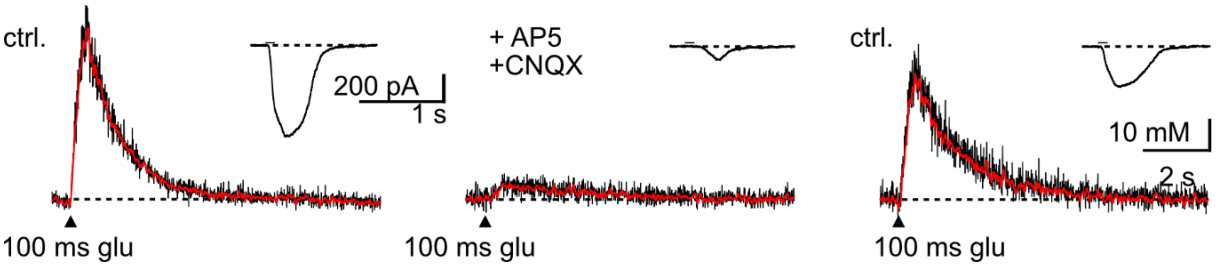

Figure 19: Pharmacology of the induced signal. Dendritic $[Na^+]_i$ transients and currents measured via the soma-based patch pipette, during glutamate iontophoresis. Both Na^+ and current traces taken under control conditions (left), after wash in of glutamate receptor blockers APV and NBQX (middle), and after washout of the blockers (right). Taken from (Nelson et al, in preparation).

7.5 Spread of Na^+ in dendrites

Due to the high frequency of the performed linescans, I was able to observe an apparent spread of Na^+ in dendrites. Similar work has also been performed on cultivated cells to enable the observation of locally restricted Ca^{2+} dynamics close to spines (Korkotian and Segal, 2006) and in dendritic microdomains (Goldberg et al., 2003). The experiments performed in this study show that Na^+ propagates through the dendrite, as $[Na^+]_i$ transients were measured in segments of interest (soi) along the dendrite (Fig. 20 A,B). Thereby, $[Na^+]_i$ amplitudes both decreased and showed a temporal delay with increasing distance to the stimulation site (Fig. 20). Reports which focused on Na^+ in lizard axons (David et al., 1997), axons and primary apical dendrites of layer 5 pyramidal neurons (Fleidervish et al., 2010; Shvartsman et al., 2021), hippocampal CA1 neurons (Mondragão et al., 2016) and astrocytic endfeet (Langer et al., 2017) also report such a decrease and shift in $[Na^+]_i$ amplitudes, which was attributed to lateral diffusion. The lateral propagation of Na^+ throughout the dendrite was observed in both primary and secondary dendrites. In all cases Na^+ propagation slowed exponentially with increasing distance from the stimulation site (Fig. 20 D red line). This is to be expected given the laws of diffusion, as $[Na^+]_i$ amplitudes, and thus concentration gradients, also decrease with increasing distance from the point of Na^+ intrusion.

Taken together, linescanning enabled the observation of $[Na^+]_i$ spread throughout the dendrite. As such, $[Na^+]_i$ amplitudes decreased and shifted, with increasing distance from the stimulation site. The data thereby shows, that Na^+ diffuses through the dendrite laterally exceeding distances of more than 40 µm from the stimulation site. This was observed both in primary and spiny secondary dendrites and emphasizes that Na^+ remains unbuffered in the cytoplasm. This calls for further investigation of dendritic Na^+ dynamics, especially considering the reported impact of spine densities on lateral diffusion (Santamaria et al., 2006, 2011).

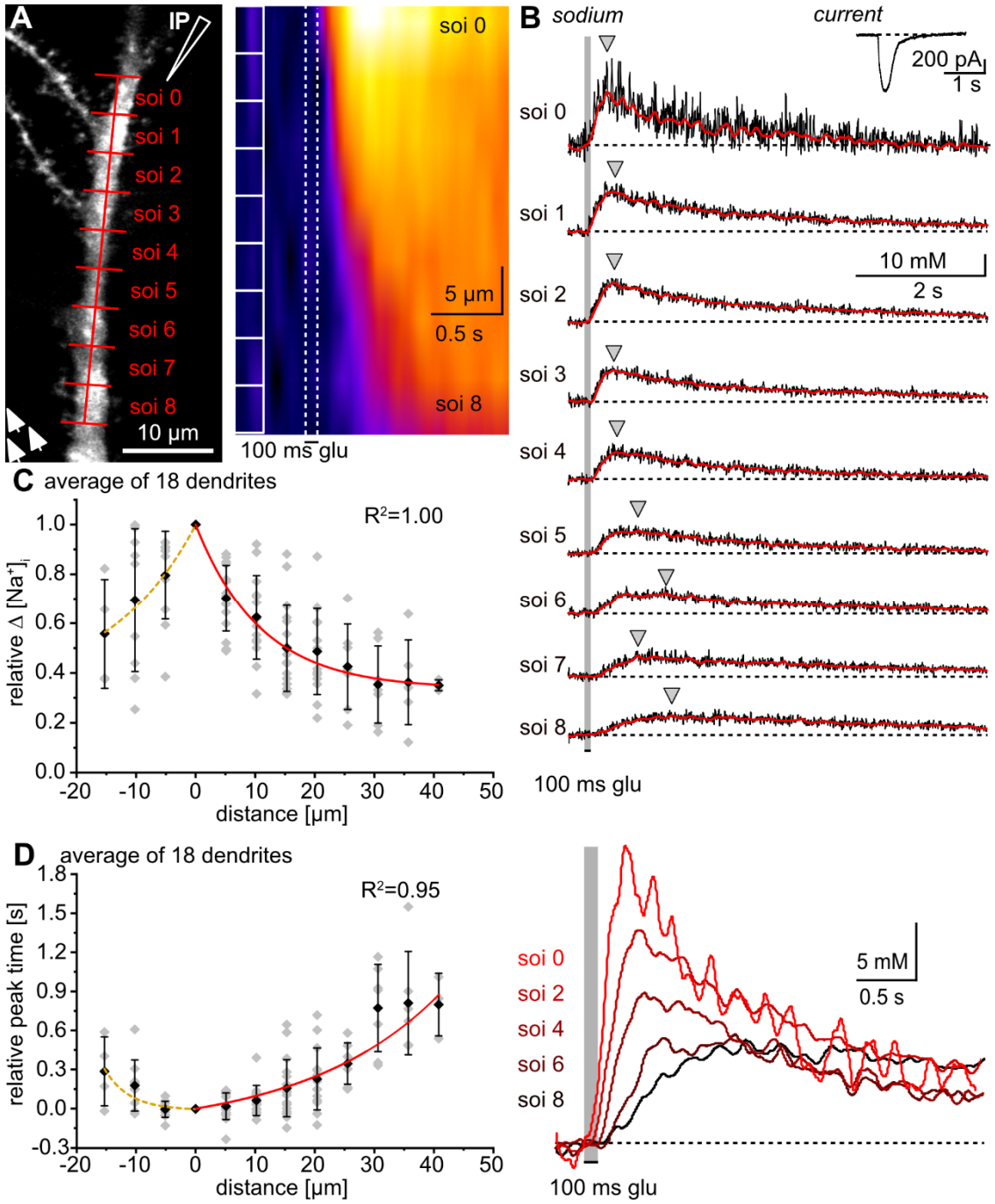

Figure 20: Spread of Na^+ through dendrites. A: Image of a primary dendrite, filled with the Na^+ indicator dye SBFI. The iontophoresis pipette (IP) is highlighted. The perfusion direction is indicated by three arrows. Left, image of the dendrite in the plane, which was used to conduct the measurement. The red line indicates the trajectory of the performed linescan with sois. Soi0 displayed the highest Na^+ amplitude and was closest to the iontophoresis pipette. Right, baseline corrected image of the linescan over time, as provided by a python-based customized program. **B:** Traces imaged at soi0 - 9 after baseline subtraction (black) and filtering (red). Grey arrows indicate the peak timepoint, which was determined by the python-based program. The grey box indicates the stimulation, given by the iontophoresis pipette. Insert depicts the current trace, which was measured at the soma via patch clamp during the experimental procedure. Below: Color coded zoom-ins of the traces taken from soi 0, soi 2, soi 4, soi 6 and soi 8. **C:** Normalized $[Na^+]_i$ amplitudes along the dendrites, plotted against their distance from soi0 taken from 18 dendrites. Plot shows data taken against the perfusion direction (positive distance), as well as with perfusion (negative distance), to show the change of $[Na^+]_i$ amplitudes in both directions. **D:** Normalized peak timepoints of $[Na^+]_i$ elevations along the dendrites, plotted against their distance from soi0 taken from n=18 dendrites. **C** and **D**: Exponential fits were fitted for data taken from sois which lay against the perfusion flow (red line). Taken from (Nelson et al, in preparation).

7.6 Coupling between dendrites and spines

After observing a lateral spread of Na^+ throughout the dendrite, I went further to establish the movement of Na^+ between spines and dendrites, thereby crossing the spine neck. Such movement has been debated throughout the last decades with reports suggesting that spines are compartmentalized from the dendrite electrically and biochemically (Araya et al., 2006; Yuste, 2013). On the other hand, previous work has proposed that such a crossing can occur for ions such as Na^+ (Miyazaki and Ross, 2017) and Ca^{2+} (Korkotian et al., 2004; Biess et al., 2007).

To further investigate the ability of Na^+ to pass into the spine head, I conducted experiments during which imaging of the dendrite and adjacent spines was performed at a distance of 14-33 µm from the iontophoresis pipette (Fig. 21 A). In this experimental setup, the occurrence of $[Na^+]_i$ signals within the spine head would be through a crossing of Na^+ from the dendrite into the spine head. The data shows that elevations of $[Na^+]_i$ occurred in both the dendrite and adjacent spine heads (Fig. 21 B,C), underlining the capability of Na^+ to readily pass through the spine neck. This is in line with previous reports, which show that Na^+ passes from the spine into the dendrite after local stimulation (Miyazaki and Ross, 2017).

Signals within the spine head were heterogenous, often showing decreased amplitudes when compared to the signals measured in dendrites (Fig. 21 D). This indicates that spines were compartmentalized from the dendrite to some extent, influencing the degree of Na^+ intrusion into the spine head. This is in line with studies, which found that the diffusion driven decay of $[Na^+]_i$ transients which were generated in the spines were heterogeneous (Miyazaki and Ross, 2022). The data also showed an increase in time constants in $[Na^+]_i$ recovery, when comparing transients in the spine to those measured in the dendrite (Fig. 21 E). This indicates that Na^+ is trapped in the spine head, again pointing to a degree of Na^+ compartmentation in the spine. A number of studies attributes such compartmental features to the morphology of the spine neck, as thin and long spine necks are related with a higher degree of compartmentation (Araya et al., 2014; Tønnesen et al., 2014). Such work also implies that the degree of compartmentation is directly linked to the strength of the synapse, as shaping of the postsynaptic spine is heavily dependent on the activation of NMDARs (Matsuzaki et al., 2004; Ultanir et al., 2007; Tønnesen et al., 2014). As a result, the resistance given by the spine neck is reduced, leading to a decreased compartmentation of the individual spine. Thus, computation of synaptic strength is conducted on the level of each individual spine which is therefore defined as the smallest computational unit of the neuron. This highly individual shaping of spine compartmentation is reflected in the heterogeneity of Na^+ movement from the dendrite into the spine head. It is therefore plausible, that spines, which are subjected to a large degree of synaptic activity, have an increased diffusional coupling with the dendrite which eases the passing of $[Na^+]_i$.

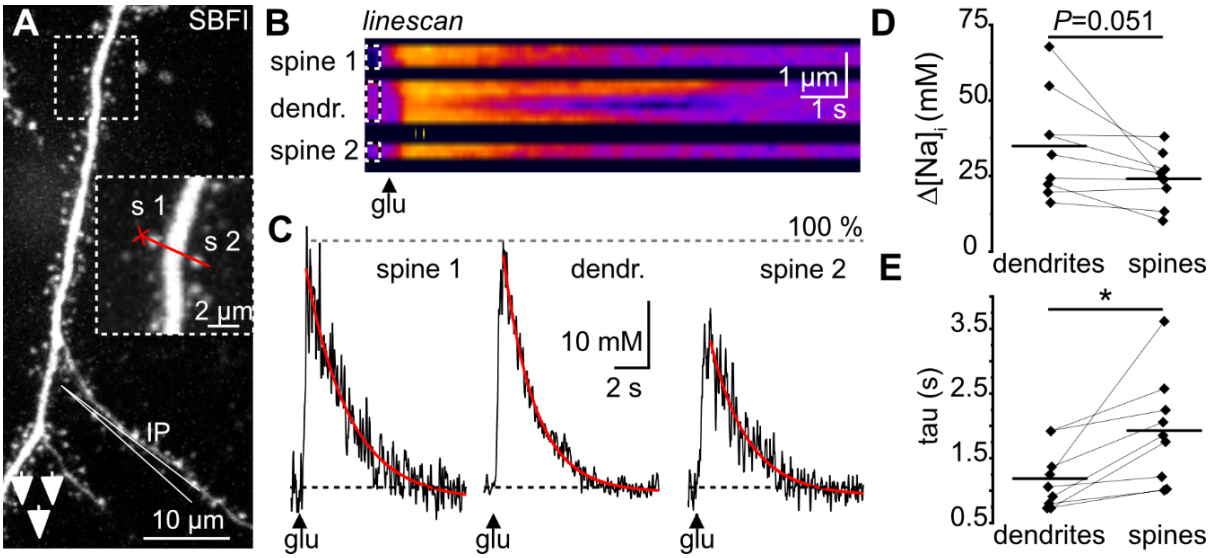

Figure 21: Diffusional coupling between the dendrite and adjacent spines. A: Maximal projection of an SBFI filled dendrite, which was used for the experimental procedure. Note that the iontophoresis pipette (IP) was placed away from the imaging site and downstream with regards to the perfusion direction (arrows). Insert shows the structure which was imaged incorporating the dendrite with adjacent spine heads (s1 and s2). The red line indicates the performed linescan with x as the starting point **B:** Image of the measured linescan over time. The spines (spine 1 and 2), as well as the dendrite are indicated in the image. **C:** Traces, taken from the dendrite, spine 1 and spine 2. Glutamate application is indicated with a black triangle. Amplitude of the dendritic signal is indicated by a dotted line, to show differences in amplitude, measured in the spines. **D:** Histogram showing the difference in amplitudes of the glutamate-induced Na+ signals, measured in 8 dendrites and 9 spines taken from 8 experiments. Means are shown as black line. Datapoints and means are connected to emphasize overall differences and differences in single experiments. **E:** Histogram, showing the difference in signal decay (τ), measured in dendrites and spines taken from 9 experiments. Taken from (Nelson et al. in preparation).

Taken together, the data shows, that Na^+ is able to pass from the dendrite into the spine head. The ability to do so is heterogeneous, which indicates that spines also display a degree of compartmentation for Na^+. Furthermore, increased recovery durations of $[Na^+]_i$ in the spine, compared to the dendrite indicate a degree of trapping and thereby at least partial compartmentation of the spine. The data therefore indicates, that spines regulate their compartmentation properties individually, which earlier reports link to the degree of synaptic activity of the spine is subjected to. The data also indicates, that Na^+ entry into one spine can pass into and thereby influence neighboring and even distant spines. This points to an active shaping of synaptic inputs postsynaptic sites of close proximity.

7.7 Characteristics of Na^+ moving through the dendrite

The data also called into question, whether characteristics of lateral Na^+ diffusion were affected by the ability of Na^+ to pass from dendrites into spine heads. Previous work has suggested a direct correlation between dendritic diffusional characteristics and the dendrite's morphology, as dendrites with a high spine density show the occurrence of anomalous diffusion. This was experimentally tested for fluorescent dextran and simulated for Cl^-

propagation through the dendrite (Santamaria et al., 2006, 2011; Mohapatra et al., 2016). The here provided work provides an experimental approach to the question how lateral Na^+ diffusion is affected. The use ORCs which were subjected to shorter or longer cultivation durations, enabled the quantification of any possible influence of the dendrite's morphology on the diffusional characteristics. For this, experiments were conducted on either primary or secondary dendrites (DIV 10-25) as well as on secondary dendrites which were subjected to either shorter (DIV 3-6) or longer cultivation durations (DIV 35-50). Primary dendrites had a significantly larger mean diameter compared to secondary dendrites. Furthermore, the mean diameter did not differ between secondary dendrites, however, spine densities were different, as DIV 3-6 secondary dendrites showed lower spine numbers than those in DIV 10-25 and DIV 35-50 ORCs (Fig. 22 A, B). This is in line with earlier reports which show that in ORCs, spine numbers increase within the first three weeks of cultivation (Buchs et al., 1993; Collin et al., 1997; De Simoni et al., 2003).

Diffusional characteristics were analyzed following previously published protocols (see Santamaria et al. 2006). Briefly, the spatial variance of the data was determined at every time point and then used to determine values for the D_{App} (Fig. 22 C,D,E). It is noteworthy, that D_{App} is commonly used to describe diffusion coefficients, which have been determined experimentally and is therefore subject to the boundaries given by the experiment (Laurent et al., 1979; Sundelöf, 1981). In this study, these included the length of the dendrite and the spread of the compound. The data which is presented in this study clearly showed a non-linear increase of spatial variance over time (Fig. 22 D). D_{App} showed a decrease over time, starting with a D_{App} of around 200 - 400 $\mu m^2\ s^{-1}$ which decreased to about 50 - 100 $\mu m^2\ s^{-1}$ after a few seconds (Fig. 22 E). Thus, the determined D_{App}s were significantly lower than D_{Na+} values which were reported in for the cytoplasmatic milieu (1500 $\mu m^2\ s^{-1}$; (Lobo, 1993), giant squid axons (1300 $\mu m^2\ s^{-1}$; (David et al., 1997)), oocytes (790 $\mu m^2\ s^{-1}$; (Allbritton et al., 1992)) or lizard muscle cells (600 $\mu m^2\ s^{-1}$; (Kushmerick and Podolsky, 1969)). Our data rather indicates, that diffusional dynamics were dampened, which has been also been assumed in studies, which simulate the effect of slow dendritic Na^+ dynamics (Zylbertal et al., 2017).

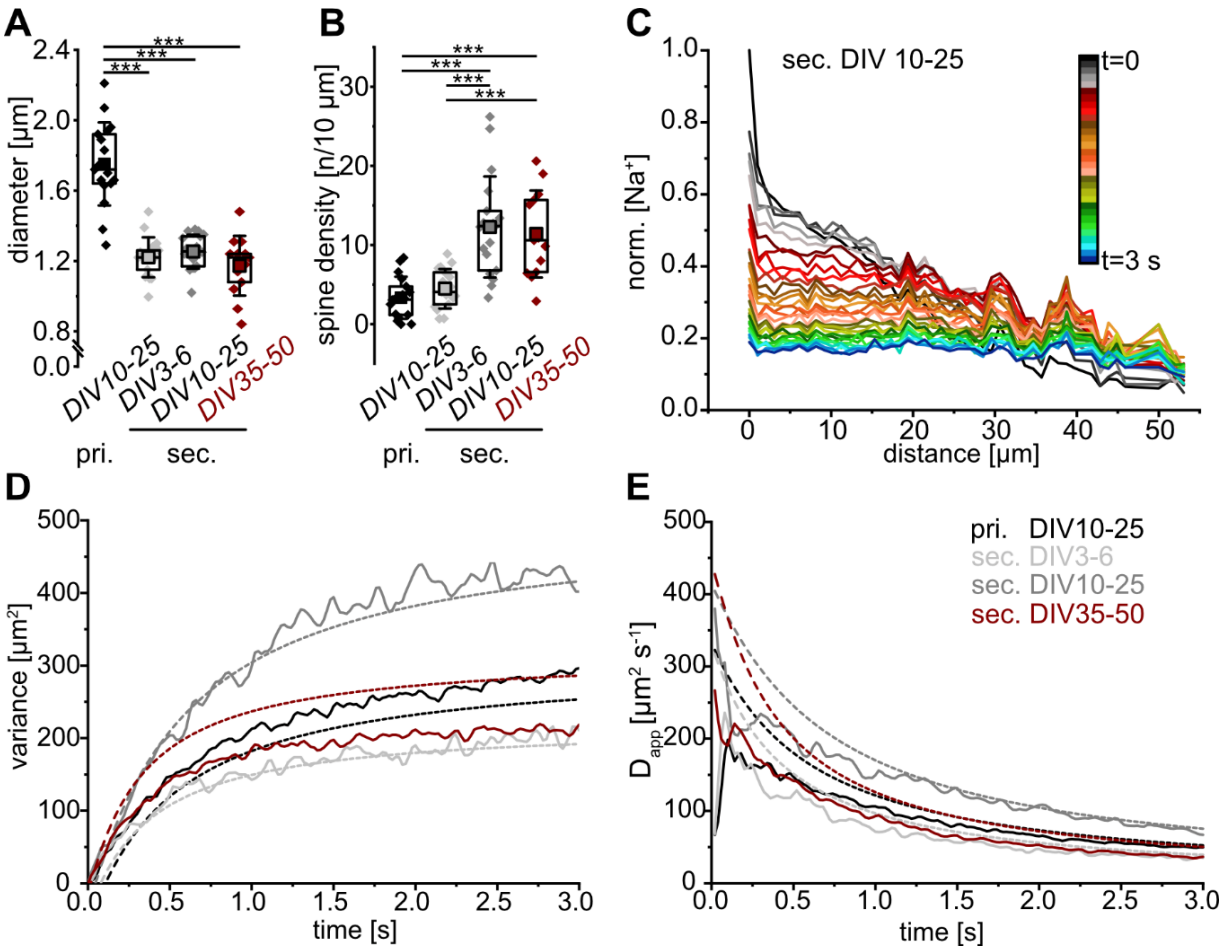

Figure 22: Diffusional characteristics of Na^+ in dendrites with varying morphologies. A, B: Boxplots comparing the dendrite diameter and spine density in primary dendrites (DIV 10-25, black diamonds) and secondary dendrites which were subjected to different cultivation periods, incorporating DIV 3-6 (n=17; light grey diamond), DIV 10-25 (n=18, dark grey diamonds) and DIV 35-54 (n=13, red diamonds). C: Concentration profiles of data taken from DIV 10-25 secondary dendrites. Spatial profiles of normalized $[Na^+]_i$ from the point of stimulation. The peak time point at the distance 0 µm is defined as t=0. For visualization purposes, the plots incorporate spatial profiles which were taken every 100 ms (10 Hz) and labelled using the inserted color code. D: The calculated spatial variance over time, calculated from profiles such as shown in C. The plot incorporates the pooled data from DIV 10-25 primary dendrites (black), DIV 3-6 secondary dendrites (bright grey), DIV 10-25 secondary dendrites (dark grey) and DIV 35-50 secondary dendrites (red). The plot also includes the outcome of simulated normal diffusion for each condition (dotted lines). E Apparent Diffusion coefficients (D_{App}) over time, resulting from variances, depicted in E. Taken from (Nelson et al, in preparation).

As D_{App} was measured experimentally, we mathematically simulated normal diffusion for all 4 samples to assess the effect of the boundary conditions given by the experiment (Fig. 22 D, E). Simulations resulted in similar trajectories for the corresponding datasets (Fig 22 D, E dotted lines), showing that $[Na^+]_i$ diffusion follows a normal diffusion process. This was also consistent among all preparations, indicating that different dendrite morphologies did not lead to a change in diffusion characteristics. This is somewhat in contrast to previous reports, which state that diffusional dynamics change depending on the spine density of the dendrite (Santamaria et al., 2006, 2011; Mohapatra et al., 2016). However, such studies report far higher dendrite densities of up to 8 spines per µm dendrite, which were not observed in this

work and which is higher than what is reported for pyramidal neurons in both cultivated, as well as acute slices (Harris and Stevens, 1989; Collin et al., 1997; Kirov et al., 1999; Pozzo-Miller et al., 1999; De Simoni et al., 2003; Konur et al., 2003; Ultanir et al., 2007; Niu et al., 2008; Perez-Cruz et al., 2011; Chapleau et al., 2012; Michaelsen-Preusse et al., 2014).

Taken together, the data shows a decrease in D_{App} which could be explained by normal diffusion. This did not differ between dendrites with different morphologies, namely dendrite diameters and spine densities, indicating that Na^+ dynamics are consistent throughout the dendritic tree. This contrasts previous reports, which state, that increased spine densities lead a dampening in diffusion of compounds and ions along the dendrite (Santamaria et al., 2006, 2011; Mohapatra et al., 2016). These experiments showed that the measured D_{App} was generally lower than previously reported coefficients which were obtained in other cellular structures (600 - 1300 $\mu m^2\ s^{-1}$), indicating a dampening of Na^+ dynamics in dendrites. Furthermore, D_{App} decreased after entering the dendrite, reaching values which are consistent with simulation studies, which propose vastly reduced Na^+ dynamics within dendrites (Zylbertal et al., 2017). As the clearance of Na^+ is heavily dependent on the dynamics of Na^+, such a reduction in Na^+ dynamics has great implications for the neuron (Zylbertal et al., 2017).

7.8 Conclusion

This work was dedicated to the analysis of intra- dendritic $[Na^+]_i$ dynamics in CA1 pyramidal neurons. Research throughout the last decade has shown that local Na^+ intrusions, which occur within the dendrite during glutamatergic synaptic transmission, are predominantly cleared away via lateral diffusion, rather than through the NKA (Mondragão et al., 2016; Miyazaki and Ross, 2017). However, other work, focusing on the general diffusion characteristics in spiny dendrites, have reported that diffusion of compounds and ions is severely dampened in dendrites (Santamaria et al., 2006, 2011; Mohapatra et al., 2016). Such a dampening generally occurs within the cytoplasm and is also influenced by the spine density. Although lateral diffusion of Na^+ through the dendrite is of such importance, studies which focus on its dynamics in dendrites are lacking. Therefore, this study was committed in investigating Na^+ dynamics in the dendrite, including the determination of dendritic $[Na^+]_i$, diffusional spread through the dendrite and the ability for Na^+ to move from the dendrite into adjacent spines.

This study therefore offers measurements of dendritic baseline $[Na^+]_i$ which were taken from both primary and secondary dendrites in the apical dendritic tree of CA1 pyramidal neurons. $[Na^+]_i$ of around 9.5 mM was consistent throughout measured dendrites and decreased to 5.3 mM upon TTX mediated silencing. Therefore, this work shows that dendritic $[Na^+]_i$ is highly influenced by neuronal activity and reflects the ability of electrochemical signals

to induce transient $[Na^+]_i$ increases. Interestingly, the TTX dependent reduction of baseline $[Na^+]_i$ has not been reported in studies, which focus upon the soma. This emphasizes the need for further studies which conduct extensive research of ion dynamics within the dendritic tree, which is directly subjected to affected by synaptic transmission as opposed to the soma.

This study focusses on the lateral diffusion of Na^+ through dendrites and determined diffusional characteristics. Experimentally determined D_{App} decreases from initial values of around 200 - 400 $\mu m^2\ s^{-1}$ to 50 – 100 $\mu m^2\ s^{-1}$ after 2 s. The dampening of Na^+ diffusion has severe physiological implications, as a reduction of diffusional dynamics lead to a prolonged Na^+ accumulation in the dendrite. Simulation studies have proposed that prolonged elevations in $[Na^+]_i$ in dendrites of pyramidal neurons due to the dampening of Na^+ diffusion have multiple resulting effects, including a reduction of EPSPs due to a shift in the Nernst potential, an increase in the NKA activity, and a Na^+-dependent increase of Ca^{2+}, due to the reversal of the NCX (Zylbertal et al., 2015; Zylbertal et al., 2017). Experimental data further the notion that prolonged accumulations of $[Na^+]_i$ have an effect on the dynamics of Ca^{2+}-signals, indicating that Ca^{2+} intrusion follows the occurrence of Na^+ spikes (Jaffe et al., 1992) due to the reversal of the NCX. Further work, focusing on the experimental verification of the simulated data is needed to fully understand the effect of the here reported dampening of Na^+ diffusion in dendrites.

This study further shows that lateral Na^+ diffusion is not affected by morphological differences of the dendrites. This agrees with work which shows that the dendritic diameter has no effect on lateral diffusion (Santamaria et al., 2006). However, the data also shows that increased spine densities did not lead to an altering of Na^+ diffusion, which is in contrast to previous publications which report a spine density dependent dampening of diffusion coefficients (Santamaria et al., 2006, 2011; Mohapatra et al., 2016). The here provided data therefore shows, that diffusional characteristics of Na^+ are not dependent on morphological attributes of the dendrite. To further verify the result, research must be undertaken which assesses dendrites with higher spine densities than those, which were reported in this study. Studies, which report a spine density dependent change in diffusional dynamics thereby use models which exceed 5 – 8 spines per µm (Santamaria et al., 2006, 2011; Mohapatra et al., 2016). Modeling the influence of such spine numbers on the propagation of Na^+ could further our understanding similar to work conducted for Cl^- (Mohapatra et al., 2016).

This study also shows that Na^+ is able to pass from dendrites into adjacent spines. The ability to do so is heterogenous, with $[Na^+]_i$ transients in spines often showing reduced amplitudes and prolonged recovery durations when compared to corresponding dendritic $[Na^+]_i$ transients. This study therefore indicates, that although Na^+ is able to pass between the dendrite and adjacent spines, its ability to do so is governed individually. This points to the processing capability of the individual spine, which are described as smallest computation unit

of the neuron (Harris and Kater, 1994; Shepherd, 1996). Many studies have attributed the compartmentation properties of spines with the spine morphology, namely the diameter of the spine neck (Svoboda et al., 1996; Noguchi et al., 2005; Holcman and Schuss, 2011; Tønnesen et al., 2014). Such studies have assessed compartmentation properties, by either the dynamics of large fluorescent molecules such as Alexa 488 or by conducting $[Ca^{2+}]_i$ measurements in dendrites and spines. Future work is needed to establish the effect of the spine's morphology on the ability for Na^+ to pass into the spine head. Such work may include measurements of $[Na^+]_i$ in dendrites and spines, coupled to STED imaging of the spine to assure sufficient resolution of the spines morphology (Nägerl et al., 2008; Tønnesen et al., 2014).

Taken together, the data presented in this study show the complex facets of Na^+ dynamics in dendrites of the apical dendritic tree of CA1 pyramidal neurons. Thereby this PhD thesis provides a study of Na^+ dynamics in apical dendrites, including the determination of dendritic $[Na^+]_i$, the verification of lateral diffusion through primary and secondary dendrites, the proof of the ability for Na^+ to cross between dendrite and spine head and the characterization of diffusional characteristics in dendrites with varying morphologies.

8. Publications and Manuscripts

8.1 Published manuscripts

Pages 44 - 70

Cortical brain organoid slices (cBOS) for the study of human neural cells in minimal networks

Laura Petersilie, Sonja Heiduschka, **Joel S. E. Nelson**, Louis A. Neu, Stephanie Le, Ruchika Anand, Karl W. Kafitz, Alessandro Prigione, Christine R. Rose

Published in Cell Press: iScience

DOI: https://doi.org/10.1016/j.isci.2024.109415

Impact factor: 6.107

I performed

- All patch clamp experiments and analysis, illustrated in Figure 5

My contribution to the Publication:

- Drafting and Revision of the manuscript and Figures

8.2 Manuscript under Revision in Cell Reports

Pages 72-111

Atypical plume-like events drive glutamate accumulation in metabolic stress conditions

Tim Ziebarth; Nils Pape**; Joel S. E. Nelson**; Fleur I.M. van Alphen; Manu Kalia; Hil G.E. Meijer; Christine R. Rose; Andreas Reiner

Submitted to Cell report (on the 15th May,2024)

Impact factor: 9.995

In accordance with both appraisers, the manuscript, which is currently under revision, is not attached in this version of the dissertation.

Upon request, the manuscript will be made assessable.

My contribution to the Manuscript

- Teaching of the methods necessary for the generation of organotypic slice cultures
- Drafting and Revision of the manuscript and Figures

8.3 Manuscript in preparation

Pages 113 - 126

$[Na^+]_i$ dynamics within dendrites of CA1 pyramidal neurons

Joel S. E. Nelson and Jan Meyer, Niklas J. Gerkau, Fidel. Santamaria and Christine R. Rose

Expected submission in 08/2024 in J Neuroscience

Impact factor: 5.3

I performed:

- Experiments which are illustrated in Figures 2-5 and in supplementary Figure 1 and 2

My contribution to the Manuscript

- The experimental design
- Analysis and interpretation of the data
- Writing of the parts “Materials and methods”, “Results” and “Discussion”
- Drafting and Revision of the manuscript and Figures

9. References

Ackermann M, Matus A (2003) Activity-induced targeting of profilin and stabilization of dendritic spine morphology. Nature neuroscience 6:1194-1200.

Allbritton NL, Meyer T, Stryer L (1992) Range of messenger action of calcium ion and inositol 1, 4, 5-trisphosphate. Science 258:1812-1815.

Andersen P (1990) Chapter synaptic integration in hippocampal CA1 pyramids. Progress in brain research 83:215-222.

Araque A, Parpura V, Sanzgiri RP, Haydon PG (1999) Tripartite synapses: glia, the unacknowledged partner. Trends in neurosciences 22:208-215.

Araya R, Eisenthal KB, Yuste R (2006) Dendritic spines linearize the summation of excitatory potentials. Proceedings of the National Academy of Sciences 103:18799-18804.

Araya R, Vogels TP, Yuste R (2014) Activity-dependent dendritic spine neck changes are correlated with synaptic strength. Proceedings of the National Academy of Sciences 111:E2895-E2904.

Araya R, Nikolenko V, Eisenthal KB, Yuste R (2007) Sodium channels amplify spine potentials. Proceedings of the National Academy of Sciences 104:12347-12352.

Arellano JI, Benavides-Piccione R, DeFelipe J, Yuste R (2007) Ultrastructure of dendritic spines: correlation between synaptic and spine morphologies. Frontiers in neuroscience 1:10.

Azarias G, Kruusmägi M, Connor S, Akkuratov EE, Liu X-L, Lyons D, Brismar H, Broberger C, Aperia A (2013) A specific and essential role for Na, K-ATPase α3 in neurons co-expressing α1 and α3. Journal of Biological Chemistry 288:2734-2743.

Bahr BA, Neve RL, Sharp J, Geller AI, Lynch G (1994) Rapid and stable gene expression in hippocampal slice cultures from a defective HSV-1 vector. Molecular brain research 26:277-285.

Ballerini L, Bracci E, Nistri A (1995) Desensitization of AMPA receptors limits the amplitude of EPSPs and the excitability of motoneurons of the rat isolated spinal cord. European Journal of Neuroscience 7:1229-1234.

Banks DS, Fradin C (2005) Anomalous diffusion of proteins due to molecular crowding. Biophysical journal 89:2960-2971.

Bannister N, Larkman A (1995a) Dendritic morphology of CA1 pyramidal neurones from the rat hippocampus: I. Branching patterns. Journal of Comparative Neurology 360:150-160.

Bannister N, Larkman A (1995b) Dendritic morphology of CA1 pyramidal neurones from the rat hippocampus: II. Spine distributions. Journal of Comparative Neurology 360:161-171.

Bardin J (2012) Making connections: Is a project to map the brain's full communications network worth the money? Nature 483:394-397.

Baum M, Erdel F, Wachsmuth M, Rippe K (2014) Retrieving the intracellular topology from multi-scale protein mobility mapping in living cells. Nature communications 5:4494.

Becker W (2015) Advanced time-correlated single photon counting applications: Springer.

Bennay M, Langer J, Meier SD, Kafitz KW, Rose CR (2008) Sodium signals in cerebellar Purkinje neurons and Bergmann glial cells evoked by glutamatergic synaptic transmission. Glia 56:1138-1149.

Bernardinelli Y, Salmon C, Jones EV, Farmer WT, Stellwagen D, Murai KK (2011) Astrocytes display complex and localized calcium responses to single-neuron stimulation in the hippocampus. Journal of Neuroscience 31:8905-8919.

Biess A, Korkotian E, Holcman D (2007) Diffusion in a dendritic spine: the role of geometry. Physical Review E 76:021922.

Biess A, Korkotian E, Holcman D (2011) Barriers to diffusion in dendrites and estimation of calcium spread following synaptic inputs. PLoS computational biology 7:e1002182.

Blaustein MP (2010) Sodium/calcium exchange. In: Handbook of Cell Signaling, pp 949-953: Elsevier.

Blom H, Bernhem K, Brismar H (2016) Sodium pump organization in dendritic spines. Neurophotonics 3:041803-041803.

Blom H, Rönnlund D, Scott L, Spicarova Z, Widengren J, Bondar A, Aperia A, Brismar H (2011) Spatial distribution of Na+-K+-ATPase in dendritic spines dissected by nanoscale superresolution STED microscopy. BMC neuroscience 12:1-7.

Bloodgood BL, Sabatini BL (2005) Neuronal activity regulates diffusion across the neck of dendritic spines. Science 310:866-869.

Bloodgood BL, Giessel AJ, Sabatini BL (2009) Biphasic synaptic Ca influx arising from compartmentalized electrical signals in dendritic spines. PLoS biology 7:e1000190.

Buchs P-A, Stoppini L, Muller D (1993) Structural modifications associated with synaptic development in area CA1 of rat hippocampal organotypic cultures. Developmental brain research 71:81-91.

Byrne MJ, Waxham MN, Kubota Y (2011) The impacts of geometry and binding on CaMKII diffusion and retention in dendritic spines. Journal of computational neuroscience 31:1-12.
Calabresi P, Pisani A, Mercuri N, Bernardi G (1992) Long-term potentiation in the striatum is unmasked by removing the voltage-dependent magnesium block of NMDA receptor channels. European Journal of Neuroscience 4:929-935.
Canepari M, Ross WN (2024) Spatial and temporal aspects of neuronal calcium and sodium signals measured with low-affinity fluorescent indicators. Pflügers Archiv-European Journal of Physiology 476:39-48.
Chapleau CA, Boggio EM, Calfa G, Percy AK, Giustetto M, Pozzo-Miller L (2012) Hippocampal CA1 pyramidal neurons of Mecp2 mutant mice show a dendritic spine phenotype only in the presymptomatic stage. Neural plasticity 2012.
Choi DW, Rothman SM (1990) The role of glutamate neurotoxicity in hypoxic-ischemic neuronal death. Annual review of neuroscience 13:171-182.
Coelho-Santos V, Berthiaume A-A, Ornelas S, Stuhlmann H, Shih AY (2021) Imaging the construction of capillary networks in the neonatal mouse brain. Proceedings of the National Academy of Sciences 118:e2100866118.
Colbert CM, Johnston D (1996) Axonal action-potential initiation and Na+ channel densities in the soma and axon initial segment of subicular pyramidal neurons. Journal of Neuroscience 16:6676-6686.
Collin C, Miyaguchi K, Segal M (1997) Dendritic spine density and LTP induction in cultured hippocampal slices. Journal of neurophysiology 77:1614-1623.
Crank J (1979) The mathematics of diffusion: Oxford university press.
Dailey ME, Smith SJ (1996) The dynamics of dendritic structure in developing hippocampal slices. Journal of Neuroscience 16:2983-2994.
Danbolt NC (2001) Glutamate uptake. Progress in neurobiology 65:1-105.
Das S, Sasaki YF, Rothe T, Premkumar LS, Takasu M, Crandall JE, Dikkes P, Conner DA, Rayudu PV, Cheung W (1998) Increased NMDA current and spine density in mice lacking the NMDA receptor subunit NR3A. Nature 393:377-381.
Dauty E, Verkman A (2005) Actin cytoskeleton as the principal determinant of size-dependent DNA mobility in cytoplasm: a new barrier for non-viral gene delivery. Journal of Biological Chemistry 280:7823-7828.
David G, Barrett JN, Barrett EF (1997) Spatiotemporal gradients of intra-axonal [Na+] after transection and resealing in lizard peripheral myelinated axons. The Journal of physiology 498:295-307.
De Simoni A, Griesinger CB, Edwards FA (2003) Development of rat CA1 neurones in acute versus organotypic slices: role of experience in synaptic morphology and activity. The Journal of physiology 550:135-147.
DeFelipe J (2011) The evolution of the brain, the human nature of cortical circuits, and intellectual creativity. Frontiers in neuroanatomy 5:29.
DeFelipe J, Fariñas I (1992) The pyramidal neuron of the cerebral cortex: morphological and chemical characteristics of the synaptic inputs. Progress in neurobiology 39:563-607.
Deitmer JW, Ellis D (1980) The intracellular sodium activity of sheep heart Purkinje fibres: effects of local anaesthetics and tetrodotoxin. The Journal of Physiology 300:269-282.
Di Rienzo C, Gratton E, Beltram F, Cardarelli F (2015) Probing short-range protein Brownian motion in the cytoplasm of living cells. Biophysical Journal 108:324a.
Diarra A, Sheldon C, Church J (2001) In situ calibration and [H+] sensitivity of the fluorescent Na+ indicator SBFI. American Journal of Physiology-Cell Physiology.
Dietz RM, Kiedrowski L, Shuttleworth CW (2007) Contribution of Na+/Ca2+ exchange to excessive Ca2+ loading in dendrites and somata of CA1 neurons in acute slice. Hippocampus 17:1049-1059.
Dix JA, Verkman A (2008) Crowding effects on diffusion in solutions and cells. Annu Rev Biophys 37:247-263.
Donoso P, Mill J, O'Neill S, Eisner D (1992) Fluorescence measurements of cytoplasmic and mitochondrial sodium concentration in rat ventricular myocytes. The Journal of physiology 448:493-509.
Edwards AM, Phillips RA, Watkins NW, Freeman MP, Murphy EJ, Afanasyev V, Buldyrev SV, da Luz MG, Raposo EP, Stanley HE (2007) Revisiting Lévy flight search patterns of wandering albatrosses, bumblebees and deer. Nature 449:1044-1048.
Einstein A (2005) Über die von der molekularkinetischen Theorie der Wärme geforderte Bewegung von in ruhenden Flüssigkeiten suspendierten Teilchen [AdP 17, 549 (1905)]. Annalen der Physik 517:182-193.

Engert F, Bonhoeffer T (1999) Dendritic spine changes associated with hippocampal long-term synaptic plasticity. Nature 399:66-70.
Everaerts K, Thapaliya P, Pape N, Durry S, Eitelmann S, Roussa E, Ullah G, Rose CR (2023) Inward Operation of Sodium-Bicarbonate Cotransporter 1 Promotes Astrocytic Na+ Loading and Loss of ATP in Mouse Neocortex during Brief Chemical Ischemia. Cells 12:2675.
Fiala JC, Harris KM (1999) Dendrite structure. Dendrites 2:1-11.
Fick A (1855) Ueber diffusion. Annalen der Physik 170:59-86.
Filipis L, Canepari M (2021) Optical measurement of physiological sodium currents in the axon initial segment. The Journal of Physiology 599:49-66.
Fleidervish IA, Lasser-Ross N, Gutnick MJ, Ross WN (2010) Na+ imaging reveals little difference in action potential–evoked Na+ influx between axon and soma. Nature Neuroscience 13:852.
Gähwiler B (1981) Organotypic monolayer cultures of nervous tissue. Journal of neuroscience methods 4:329-342.
Gähwiler B (1984a) Slice cultures of cerebellar, hippocampal and hypothalamic tissue. Experientia 40:235-243.
Gähwiler B (1984b) Development of the hippocampus in vitro: cell types, synapses and receptors. Neuroscience 11:751-760.
Gähwiler B (1988) Organotypic cultures of neural tissue. Trends in neurosciences 11:484-489.
Gerkau NJ, Rakers C, Petzold GC, Rose CR (2017a) Differential effects of energy deprivation on intracellular sodium homeostasis in neurons and astrocytes. Journal of neuroscience research.
Gerkau NJ, Rakers C, Durry S, Petzold GC, Rose CR (2017b) Reverse NCX attenuates cellular sodium loading in metabolically compromised cortex. Cerebral Cortex 28:4264-4280.
Gerkau NJ, Lerchundi R, Nelson JS, Lantermann M, Meyer J, Hirrlinger J, Rose CR (2019) Relation between activity-induced intracellular sodium transients and ATP dynamics in mouse hippocampal neurons. The Journal of physiology.
Giandomenico SL, Sutcliffe M, Lancaster MA (2021) Generation and long-term culture of advanced cerebral organoids for studying later stages of neural development. Nature protocols 16:579-602.
Giandomenico SL, Mierau SB, Gibbons GM, Wenger LM, Masullo L, Sit T, Sutcliffe M, Boulanger J, Tripodi M, Derivery E (2019) Cerebral organoids at the air–liquid interface generate diverse nerve tracts with functional output. Nature neuroscience 22:669-679.
Giesing M, Neumann G, Egge H, Zilliken F (1975) Lipid Metabolism of Developing Central Nervous Tissues in Organotypic Cultures: I. Lipid Distribution and Fatty Acid Profiles of the Medium for Rat Brain Cortex in vitro. Annals of Nutrition and Metabolism 19:242-250.
Goldberg JH, Tamas G, Aronov D, Yuste R (2003) Calcium microdomains in aspiny dendrites. Neuron 40:807-821.
Golding NL, Spruston N (1998) Dendritic sodium spikes are variable triggers of axonal action potentials in hippocampal CA1 pyramidal neurons. Neuron 21:1189-1200.
Golding NL, Mickus TJ, Katz Y, Kath WL, Spruston N (2005) Factors mediating powerful voltage attenuation along CA1 pyramidal neuron dendrites. The Journal of physiology 568:69-82.
Goldman DE (1943) Potential, impedance, and rectification in membranes. The Journal of general physiology 27:37-60.
Gray EG (1959) Electron microscopy of synaptic contacts on dendrite spines of the cerebral cortex. Nature 183:1592.
Grynkiewicz G, Poenie M, Tsien RY (1985) A new generation of Ca2+ indicators with greatly improved fluorescence properties. Journal of biological chemistry 260:3440-3450.
Haack N, Durry S, Kafitz KW, Chesler M, Rose CR (2015) Double-barreled and concentric microelectrodes for measurement of extracellular ion signals in brain tissue. JoVE (Journal of Visualized Experiments):e53058.
Haber M, Zhou L, Murai KK (2006) Cooperative astrocyte and dendritic spine dynamics at hippocampal excitatory synapses. Journal of Neuroscience 26:8881-8891.
Hardingham GE, Bading H (1999) Calcium as a versatile second messenger in the control of gene expression. Microscopy research and technique 46:348-355.
Harootunian A, Kao J, Eckert B, Tsien R (1989) Fluorescence ratio imaging of cytosolic free Na+ in individual fibroblasts and lymphocytes. Journal of Biological Chemistry 264:19458-19467.
Harrington MG, Salomon RM, Pogoda JM, Oborina E, Okey N, Johnson B, Schmidt D, Fonteh AN, Dalleska NF (2010) Cerebrospinal fluid sodium rhythms. Cerebrospinal fluid research 7:1-9.
Harris E, Witter MP, Weinstein G, Stewart M (2001) Intrinsic connectivity of the rat subiculum: I. Dendritic morphology and patterns of axonal arborization by pyramidal neurons. Journal of Comparative Neurology 435:490-505.

Harris KM, Stevens JK (1989) Dendritic spines of CA 1 pyramidal cells in the rat hippocampus: serial electron microscopy with reference to their biophysical characteristics. Journal of Neuroscience 9:2982-2997.
Harris KM, Kater S (1994) Dendritic spines: cellular specializations imparting both stability and flexibility to synaptic function. Annual review of neuroscience 17:341-371.
Harris KM, Jensen FE, Tsao B (1992) Three-dimensional structure of dendritic spines and synapses in rat hippocampus (CA1) at postnatal day 15 and adult ages: implications for the maturation of synaptic physiology and long-term potentiation [published erratum appears in J Neurosci 1992 Aug; 12 (8): following table of contents]. Journal of Neuroscience 12:2685-2705.
Hering H, Sheng M (2001) Dentritic spines: structure, dynamics and regulation. Nature Reviews Neuroscience 2:880-888.
Hertz L (1979) Functional interactions between neurons and astrocytes I. Turnover and metabolism of putative amino acid transmitters. Progress in neurobiology 13:277-323.
Hille B (2011) Ionic basis of resting and action potentials. Comprehensive Physiology:99-136.
Hodgkin AL, Katz B (1949) The effect of sodium ions on the electrical activity of the giant axon of the squid. The Journal of physiology 108:37-77.
Holcman D, Schuss Z (2011) Diffusion laws in dendritic spines. The Journal of Mathematical Neuroscience 1:1-14.
Holcman D, Yuste R (2015) The new nanophysiology: regulation of ionic flow in neuronal subcompartments. Nature Reviews Neuroscience 16:685-692.
Holmes JR, Berkowitz A (2014) Dendritic orientation and branching distinguish a class of multifunctional turtle spinal interneurons. Frontiers in Neural Circuits 8:136.
Humpel C (2015) Organotypic brain slice cultures: A review. Neuroscience 305:86-98.
Ikegaya Y, Le Bon-Jego M, Yuste R (2005) Large-scale imaging of cortical network activity with calcium indicators. Neuroscience research 52:132-138.
Ilouz R, Lev-Ram V, Bushong EA, Stiles TL, Friedmann-Morvinski D, Douglas C, Goldberg JL, Ellisman MH, Taylor SS (2017) Isoform-specific subcellular localization and function of protein kinase A identified by mosaic imaging of mouse brain. Elife 6:e17681.
Ishikawa T, Ishikawa AW, Papoutsi A, Tanimura A, Yonehara K (2023) Subcellular computations and information processing. In, p 1169671: Frontiers Media SA.
Jaffe DB, Johnston D, Lasser-Ross N, Lisman JE, Miyakawa H, Ross WN (1992) The spread of Na+ spikes determines the pattern of dendritic Ca2+ entry into hippocampal neurons. Nature 357:244.
Jayant K, Hirtz JJ, Jen-La Plante I, Tsai DM, De Boer WD, Semonche A, Peterka DS, Owen JS, Sahin O, Shepard KL (2017) Targeted intracellular voltage recordings from dendritic spines using quantum-dot-coated nanopipettes. Nature nanotechnology 12:335.
Jourdain P, Fukunaga K, Muller D (2003) Calcium/calmodulin-dependent protein kinase II contributes to activity-dependent filopodia growth and spine formation. Journal of Neuroscience 23:10645-10649.
Karus C, Mondragão MA, Ziemens D, Rose CR (2015) Astrocytes restrict discharge duration and neuronal sodium loads during recurrent network activity. Glia 63:936-957.
Kelly T, Rose CR (2010) Ammonium influx pathways into astrocytes and neurones of hippocampal slices. Journal of neurochemistry 115:1123-1136.
Kirischuk S, Parpura V, Verkhratsky A (2012) Sodium dynamics: another key to astroglial excitability? Trends in neurosciences 35:497-506.
Kirov SA, Sorra KE, Harris KM (1999) Slices have more synapses than perfusion-fixed hippocampus from both young and mature rats. Journal of Neuroscience 19:2876-2886.
Klafter J, Sokolov IM (2005) Anomalous diffusion spreads its wings. Physics world 18:29.
Knöpfel T, Anchisi D, Alojado M, Tempia F, Strata P (2000) Elevation of intradendritic sodium concentration mediated by synaptic activation of metabotropic glutamate receptors in cerebellar Purkinje cells. European Journal of Neuroscience 12:2199-2204.
Konur S, Rabinowitz D, Fenstermaker VL, Yuste R (2003) Systematic regulation of spine sizes and densities in pyramidal neurons. Journal of neurobiology 56:95-112.
Korkotian E, Segal M (2006) Spatially confined diffusion of calcium in dendrites of hippocampal neurons revealed by flash photolysis of caged calcium. Cell calcium 40:441-449.
Korkotian E, Holcman D, Segal M (2004) Dynamic regulation of spine–dendrite coupling in cultured hippocampal neurons. European Journal of Neuroscience 20:2649-2663.
Korogod N, Petersen CC, Knott GW (2015) Ultrastructural analysis of adult mouse neocortex comparing aldehyde perfusion with cryo fixation. Elife 4:e05793.

Kupper J, Ascher P, Neyton J (1998) Internal Mg2+ block of recombinant NMDA channels mutated within the selectivity filter and expressed in Xenopus oocytes. The Journal of Physiology 507:1-12.
Kushmerick M, Podolsky R (1969) Ionic mobility in muscle cells. Science 166:1297-1298.
Kusumi A, Sako Y, Yamamoto M (1993) Confined lateral diffusion of membrane receptors as studied by single particle tracking (nanovid microscopy). Effects of calcium-induced differentiation in cultured epithelial cells. Biophysical journal 65:2021-2040.
Lamy CM, Chatton J-Y (2011) Optical probing of sodium dynamics in neurons and astrocytes. Neuroimage 58:572-578.
Langer J, Rose CR (2009) Synaptically induced sodium signals in hippocampal astrocytes in situ. The Journal of physiology 587:5859-5877.
Langer J, Gerkau NJ, Derouiche A, Kleinhans C, Moshrefi-Ravasdjani B, Fredrich M, Kafitz KW, Seifert G, Steinhäuser C, Rose CR (2017) Rapid sodium signaling couples glutamate uptake to breakdown of ATP in perivascular astrocyte endfeet. Glia 65:293-308.
Langhammer CG, Previtera ML, Sweet ES, Sran SS, Chen M, Firestein BL (2010) Automated Sholl analysis of digitized neuronal morphology at multiple scales: whole cell Sholl analysis versus Sholl analysis of arbor subregions. Cytometry Part A 77:1160-1168.
Lasser-Ross N, Ross WN (1992) Imaging voltage and synaptically activated sodium transients in cerebellar Purkinje cells. Proceedings of the Royal Society of London Series B: Biological Sciences 247:35-39.
Laurent T, Preston B, Sundelöf L-O (1979) Transport of molecules in concentrated systems. Nature 279:60-62.
Lee J-M, Zipfel GJ, Choi DW (1999) The changing landscape of ischaemic brain injury mechanisms. Nature 399:A7.
Lerchundi R, Kafitz KW, Winkler U, Färfers M, Hirrlinger J, Rose CR (2019) FRET-based imaging of intracellular ATP in organotypic brain slices. Journal of neuroscience research 97:933-945.
Liebmann T, Blom H, Aperia A, Brismar H (2013) Nanoscale elucidation of Na, K-ATPase isoforms in dendritic spines. Optical Nanoscopy 2:1-10.
Lobo VM (1993) Mutual diffusion coefficients in aqueous electrolyte solutions (technical report). Pure and applied chemistry 65:2613-2640.
Ma T, Matveev VS, Pavlyukevich I (2021) Geodesic random walks, diffusion processes and Brownian motion on Finsler manifolds. The Journal of Geometric Analysis 31:12446-12484.
MacKintosh FC (2012) Active diffusion: the erratic dance of chromosomal loci. Proceedings of the National Academy of Sciences 109:7138-7139.
Magee JC (2000) Dendritic integration of excitatory synaptic input. Nature Reviews Neuroscience 1:181-190.
Majewska A, Tashiro A, Yuste R (2000) Regulation of spine calcium dynamics by rapid spine motility. Journal of Neuroscience 20:8262-8268.
Maletic-Savatic M, Malinow R, Svoboda K (1999) Rapid dendritic morphogenesis in CA1 hippocampal dendrites induced by synaptic activity. Science 283:1923-1927.
Malinow R, Malenka RC (2002) AMPA receptor trafficking and synaptic plasticity. Annual review of neuroscience 25:103-126.
Mancuso JJ, Chen Y, Li X, Xue Z, Wong ST (2013) Methods of dendritic spine detection: from Golgi to high-resolution optical imaging. Neuroscience 251:129-140.
Matsuoka S, Nicoll DA, He Z, Philipson KD (1997) Regulation of the cardiac Na+-Ca2+ exchanger by the endogenous XIP region. The Journal of general physiology 109:273-286.
Matsuzaki M, Honkura N, Ellis-Davies GC, Kasai H (2004) Structural basis of long-term potentiation in single dendritic spines. Nature 429:761-766.
Megıas M, Emri Z, Freund T, Gulyas A (2001) Total number and distribution of inhibitory and excitatory synapses on hippocampal CA1 pyramidal cells. Neuroscience 102:527-540.
Meier SD, Kovalchuk Y, Rose CR (2006) Properties of the new fluorescent Na+ indicator CoroNa Green: comparison with SBFI and confocal Na+ imaging. Journal of neuroscience methods 155:251-259.
Méndez V, Iomin A (2013) Comb-like models for transport along spiny dendrites. Chaos, Solitons & Fractals 53:46-51.
Meyer J, Untiet V, Fahlke C, Gensch T, Rose CR (2019) Quantitative determination of cellular [Na+] by fluorescence lifetime imaging with CoroNaGreen. Journal of General Physiology 151:1319-1331.
Meyer J, Gerkau NJ, Kafitz KW, Patting M, Jolmes F, Henneberger C, Rose CR (2022) Rapid fluorescence lifetime imaging reveals that TRPV4 channels promote dysregulation of neuronal Na+ in ischemia. Journal of Neuroscience 42:552-566.

Michaelsen-Preusse K, Kellner Y, Korte M, Zagrebelsky M (2014) Analysis of actin turnover and spine dynamics in hippocampal slice cultures. Laser Scanning Microscopy and Quantitative Image Analysis of Neuronal Tissue:189-217.
Minta A, Tsien RY (1989) Fluorescent indicators for cytosolic sodium. Journal of Biological Chemistry 264:19449-19457.
Miyazaki K, Ross WN (2015) Simultaneous sodium and calcium imaging from dendrites and axons. Eneuro 2.
Miyazaki K, Ross WN (2017) Sodium dynamics in pyramidal neuron dendritic spines: synaptically evoked entry predominantly through AMPA receptors and removal by diffusion. Journal of Neuroscience 37:9964-9976.
Miyazaki K, Ross WN (2022) Fast synaptically activated calcium and sodium kinetics in hippocampal pyramidal neuron dendritic spines. Eneuro 9.
Miyazaki K, Lisman JE, Ross WN (2019) Improvements in simultaneous sodium and calcium imaging. Frontiers in cellular neuroscience 12:514.
Mohapatra N, Tønnesen J, Vlachos A, Kuner T, Deller T, Nägerl UV, Santamaria F, Jedlicka P (2016) Spines slow down dendritic chloride diffusion and affect short-term ionic plasticity of GABAergic inhibition. Scientific reports 6:23196.
Mondragão MA, Schmidt H, Kleinhans C, Langer J, Kafitz KW, Rose CR (2016) Extrusion versus diffusion: mechanisms for recovery from sodium loads in mouse CA1 pyramidal neurons. The Journal of physiology 594:5507-5527.
Müller C, Remy S (2013) Fast micro-iontophoresis of glutamate and GABA: a useful tool to investigate synaptic integration. Journal of visualized experiments: JoVE.
Müller M, Gähwiler B, Rietschin L, Thompson SM (1993) Reversible loss of dendritic spines and altered excitability after chronic epilepsy in hippocampal slice cultures. Proceedings of the National Academy of Sciences 90:257-261.
Müller M, Somjen GG (2000) Na+ and K+ concentrations, extra-and intracellular voltages, and the effect of TTX in hypoxic rat hippocampal slices. Journal of neurophysiology 83:735-745.
Nägerl UV, Willig KI, Hein B, Hell SW, Bonhoeffer T (2008) Live-cell imaging of dendritic spines by STED microscopy. Proceedings of the National Academy of Sciences 105:18982-18987.
Nikonenko I, Nikonenko A, Mendez P, Michurina TV, Enikolopov G, Muller D (2013) Nitric oxide mediates local activity-dependent excitatory synapse development. Proceedings of the National Academy of Sciences 110:E4142-E4151.
Niu S, Yabut O, D'Arcangelo G (2008) The Reelin signaling pathway promotes dendritic spine development in hippocampal neurons. Journal of Neuroscience 28:10339-10348.
Noguchi J, Matsuzaki M, Ellis-Davies GC, Kasai H (2005) Spine-neck geometry determines NMDA receptor-dependent Ca2+ signaling in dendrites. Neuron 46:609-622.
O'Neill KM, Akum BF, Dhawan ST, Kwon M, Langhammer CG, Firestein BL (2015) Assessing effects on dendritic arborization using novel Sholl analyses. Frontiers in cellular neuroscience 9:285.
O'Brien RJ, Kamboj S, Ehlers MD, Rosen KR, Fischbach GD, Huganir RL (1998) Activity-dependent modulation of synaptic AMPA receptor accumulation. Neuron 21:1067-1078.
Okamoto K, Ishikawa T, Abe R, Ishikawa D, Kobayashi C, Mizunuma M, Norimoto H, Matsuki N, Ikegaya Y (2014) Ex vivo cultured neuronal networks emit in vivo-like spontaneous activity. The journal of physiological sciences 64:421-431.
Oschmann F, Mergenthaler K, Jungnickel E, Obermayer K (2017) Spatial separation of two different pathways accounting for the generation of calcium signals in astrocytes. PLoS computational biology 13:e1005377.
Pape N, Rose CR (2023) Activation of TRPV4 channels promotes the loss of cellular ATP in organotypic slices of the mouse neocortex exposed to chemical ischemia. The Journal of Physiology 601:2975-2990.
Parajuli LK, Urakubo H, Takahashi-Nakazato A, Ogelman R, Iwasaki H, Koike M, Kwon H-B, Ishii S, Oh WC, Fukazawa Y (2020) Geometry and the organizational principle of spine synapses along a dendrite. eneuro 7.
Perez-Cruz C, Nolte MW, van Gaalen MM, Rustay NR, Termont A, Tanghe A, Kirchhoff F, Ebert U (2011) Reduced spine density in specific regions of CA1 pyramidal neurons in two transgenic mouse models of Alzheimer's disease. Journal of Neuroscience 31:3926-3934.
Pessoa L (2014) Understanding brain networks and brain organization. Physics of life reviews 11:400-435.
Peters A, Kaiserman-Abramof IR (1970) The small pyramidal neuron of the rat cerebral cortex. The perikaryon, dendrites and spines. American Journal of Anatomy 127:321-355.

Petersilie L, Heiduschka S, Nelson JS, Neu LA, Le S, Anand R, Kafitz KW, Prigione A, Rose CR (2024) Cortical brain organoid slices (cBOS) for the study of human neural cells in minimal networks. Iscience 27.
Petrozzino JJ, Miller LDP, Connor JA (1995) Micromolar Ca2+ transients in dendritic spines of hippocampal pyramidal neurons in brain slice. Neuron 14:1223-1231.
Philipson KD, Nicoll DA (2000) Sodium-calcium exchange: a molecular perspective. Annual review of physiology 62:111-133.
Piet R, Vargová L, Syková E, Poulain DA, Oliet SH (2004) Physiological contribution of the astrocytic environment of neurons to intersynaptic crosstalk. Proceedings of the National Academy of Sciences 101:2151-2155.
Pisani A, Calabresi P, Tozzi A, Bernardi G, Knöpfel T (1998) SHORT COMUNICATIONEarly sodium elevations induced by combined oxygen and glucose deprivation in pyramidal cortical neurons. European Journal of Neuroscience 10:3572-3574.
Popov S, Poo M (1992) Diffusional transport of macromolecules in developing nerve processes. Journal of Neuroscience 12:77-85.
Pozzo-Miller LD, Inoue T, Murphy DD (1999) Estradiol increases spine density and NMDA-dependent Ca2+ transients in spines of CA1 pyramidal neurons from hippocampal slices. Journal of neurophysiology 81:1404-1411.
Qian N, Sejnowski T (1989) An electro-diffusion model for computing membrane potentials and ionic concentrations in branching dendrites, spines and axons. Biological Cybernetics 62:1-15.
Ritchie K, Shan X-Y, Kondo J, Iwasawa K, Fujiwara T, Kusumi A (2005) Detection of non-Brownian diffusion in the cell membrane in single molecule tracking. Biophysical journal 88:2266-2277.
Roder P, Hille C (2014) ANG-2 for quantitative Na+ determination in living cells by time-resolved fluorescence microscopy. Photochemical & photobiological sciences 13:1699-1710.
Roelandse M, Welman A, Wagner U, Hagmann J, Matus A (2003) Focal motility determines the geometry of dendritic spines☆. Neuroscience 121:39-49.
Rose C (2003) High-resolution Na+ imaging in dendrites and spines. Pflügers Archiv European Journal of Physiology 446:317-321.
Rose C, Chatton J-Y (2016) Astrocyte sodium signaling and neuro-metabolic coupling in the brain. Neuroscience 323:121-134.
Rose CR (1997) Intracellular Na+ regulation in neurons and glia: functional implications. The Neuroscientist 3:85-88.
Rose CR (2012) Two-photon sodium imaging in dendritic spines. Cold Spring Harbor Protocols 2012:pdb. prot072074.
Rose CR, Ransom BR (1996) Mechanisms of H+ and Na+ changes induced by glutamate, kainate, and D-aspartate in rat hippocampal astrocytes. Journal of Neuroscience 16:5393-5404.
Rose CR, Ransom BR (1997) Regulation of intracellular sodium in cultured rat hippocampal neurones. The Journal of physiology 499:573-587.
Rose CR, Konnerth A (2001) NMDA receptor-mediated Na+ signals in spines and dendrites. Journal of Neuroscience 21:4207-4214.
Rose CR, Kovalchuk Y, Eilers J, Konnerth A (1999) Two-photon Na+ imaging in spines and fine dendrites of central neurons. Pflügers Archiv 439:201-207.
Rungta RL, Choi HB, Tyson JR, Malik A, Dissing-Olesen L, Lin PJ, Cain SM, Cullis PR, Snutch TP, MacVicar BA (2015) The cellular mechanisms of neuronal swelling underlying cytotoxic edema. Cell 161:610-621.
Sah P, Hestrin S, Nicoll R (1989) Tonic activation of NMDA receptors by ambient glutamate enhances excitability of neurons. Science 246:815-818.
Sakmann B, Neher E (1984) Patch clamp techniques for studying ionic channels in excitable membranes. Annual review of physiology 46:455-472.
Santamaria F, Wils S, De Schutter E, Augustine GJ (2006) Anomalous diffusion in Purkinje cell dendrites caused by spines. Neuron 52:635-648.
Santamaria F, Wils S, De Schutter E, Augustine GJ (2011) The diffusional properties of dendrites depend on the density of dendritic spines. European Journal of Neuroscience 34:561-568.
Schiller J, Schiller Y (2001) NMDA receptor-mediated dendritic spikes and coincident signal amplification. Current opinion in neurobiology 11:343-348.
Schiller J, Schiller Y, Clapham DE (1998) NMDA receptors amplify calcium influx into dendritic spines during associative pre-and postsynaptic activation. Nature neuroscience 1:114.
Schiller J, Major G, Koester HJ, Schiller Y (2000) NMDA spikes in basal dendrites of cortical pyramidal neurons. Nature 404:285.
Segal M, Andersen P (2000) Dendritic spines shaped by synaptic activity. Current opinion in neurobiology 10:582-586.

Shepherd GM (1996) The dendritic spine: a multifunctional integrative unit. Journal of neurophysiology 75:2197-2210.
Shvartsman A, Kotler O, Stoler O, Khrapunsky Y, Melamed I, Fleidervish IA (2021) Subcellular distribution of persistent sodium conductance in cortical pyramidal neurons. Journal of Neuroscience 41:6190-6201.
Son J, Song S, Lee S, Chang S, Kim M (2011) Morphological change tracking of dendritic spines based on structural features. Journal of microscopy 241:261-272.
Sporns O (2011) The human connectome: a complex network. Annals of the new York Academy of Sciences 1224:109-125.
Spruston N (2008) Pyramidal neurons: dendritic structure and synaptic integration. Nature Reviews Neuroscience 9:206.
Spruston N, Jonas P, Sakmann B (1995) Dendritic glutamate receptor channels in rat hippocampal CA3 and CA1 pyramidal neurons. The Journal of physiology 482:325-352.
Stoppini L, Buchs P-A, Muller D (1991) A simple method for organotypic cultures of nervous tissue. Journal of neuroscience methods 37:173-182.
Sundelöf L-O (1981) Definition and interpretation of an apparent diffusion coefficient in multicomponent systems. Journal of the Chemical Society, Faraday Transactions 2: Molecular and Chemical Physics 77:1779-1781.
Svoboda K, Tank DW, Denk W (1996) Direct measurement of coupling between dendritic spines and shafts. Science 272:716-719.
Swulius MT, Kubota Y, Forest A, Waxham MN (2010) Structure and composition of the postsynaptic density during development. Journal of Comparative Neurology 518:4243-4260.
Takasaki K, Sabatini BL (2014) Super-resolution 2-photon microscopy reveals that the morphology of each dendritic spine correlates with diffusive but not synaptic properties. Frontiers in neuroanatomy 8:29.
Tian W, Peng L, Zhao M, Tao L, Zou P, Zhang Y (2022) Dendritic Morphology Affects the Velocity and Amplitude of Back-propagating Action Potentials. Neuroscience Bulletin 38:1330-1346.
Tønnesen J, Nägerl UV (2016) Dendritic spines as tunable regulators of synaptic signals. Frontiers in psychiatry 7:101.
Tønnesen J, Katona G, Rózsa B, Nägerl UV (2014) Spine neck plasticity regulates compartmentalization of synapses. Nature neuroscience 17:678.
Torp R, Haug F, Tønder N, Zimmer J, Ottersen O (1992) Neuroactive amino acids in organotypic slice cultures of the rat hippocampus: an immunocytochemical study of the distribution of GABA, glutamate, glutamine and taurine. Neuroscience 46:807-823.
Ultanir SK, Kim J-E, Hall BJ, Deerinck T, Ellisman M, Ghosh A (2007) Regulation of spine morphology and spine density by NMDA receptor signaling in vivo. Proceedings of the National Academy of Sciences 104:19553-19558.
Umemiya M, Senda M, Murphy TH (1999) Behaviour of NMDA and AMPA receptor-mediated miniature EPSCs at rat cortical neuron synapses identified by calcium imaging. The Journal of physiology 521:113-122.
Untiet V, Kovermann P, Gerkau NJ, Gensch T, Rose CR, Fahlke C (2017) Glutamate transporter-associated anion channels adjust intracellular chloride concentrations during glial maturation. Glia 65:388-400.
Verkhratsky A (2002) The endoplasmic reticulum and neuronal calcium signalling. Cell calcium 32:393-404.
Verkhratsky A, Nedergaard M (2018) Physiology of astroglia. Physiological reviews 98:239-389.
Watt AJ, van Rossum MC, MacLeod KM, Nelson SB, Turrigiano GG (2000) Activity coregulates quantal AMPA and NMDA currents at neocortical synapses. Neuron 26:659-670.
Weilinger NL, Wicki-Stordeur LE, Groten CJ, LeDue JM, Kahle KT, MacVicar BA (2022) KCC2 drives chloride microdomain formation in dendritic blebbing. Cell Reports 41.
Weiss M, Elsner M, Kartberg F, Nilsson T (2004) Anomalous subdiffusion is a measure for cytoplasmic crowding in living cells. Biophysical journal 87:3518-3524.
Williams RW, Herrup K (1988) The control of neuron number. Annual review of neuroscience 11:423-453.
Yates JL, Scholl B (2022) Unraveling Functional Diversity of Cortical Synaptic Architecture Through the Lens of Population Coding. Frontiers in Synaptic Neuroscience 14:888214.
Yuste R (2013) Electrical compartmentalization in dendritic spines. Annual review of neuroscience 36:429-449.
Yuste R, Denk W (1995) Dendritic spines as basic functional units of neuronal integration. Nature 375:682.

Zhang Z, Liu Z, Tian Y (2020) A DNA-Based FLIM reporter for simultaneous quantification of lysosomal pH and Ca2+ during autophagy regulation. Iscience 23.
Zheng K, Jensen TP, Rusakov DA (2018) Monitoring intracellular nanomolar calcium using fluorescence lifetime imaging. Nature protocols 13:581-597.
Zheng K, Bard L, Reynolds JP, King C, Jensen TP, Gourine AV, Rusakov DA (2015) Time-resolved imaging reveals heterogeneous landscapes of nanomolar Ca2+ in neurons and astroglia. Neuron 88:277-288.
Ziemens D, Oschmann F, Gerkau NJ, Rose CR (2019) Heterogeneity of activity-induced sodium transients between astrocytes of the mouse hippocampus and neocortex: Mechanisms and consequences. Journal of Neuroscience 39:2620-2634.
Ziv NE, Smith SJ (1996) Evidence for a role of dendritic filopodia in synaptogenesis and spine formation. Neuron 17:91-102.
Zylbertal A, Yarom Y, Wagner S (2017) The Slow Dynamics of Intracellular Sodium Concentration Increase the Time Window of Neuronal Integration: A Simulation Study. Frontiers in computational neuroscience 11:85.
Zylbertal A, Kahan A, Ben-Shaul Y, Yarom Y, Wagner S (2015) Prolonged intracellular Na+ dynamics govern electrical activity in accessory olfactory bulb mitral cells. PLoS biology 13:e1002319.

10. Letter of Thanks/ Danksagung

Man sagt es braucht ein Dorf um ein Kind zu erziehen. Nun ich glaube es braucht ein Institut, um einen Wissenschaftler auszubilden. Hier möchte ich mich bei meinem „Dorf“ bedanken:

Zuerst möchte ich mich mit der größtmöglichen Herzlichkeit bei Frau Prof. Dr. Christine R. Rose bedanken, die mich seit meiner Bachelorarbeit begleitet, unterstützt und gefördert hat. Bereits in der ersten Vorlesung der Neurobiologie (Bio 220) wusste ich, dass es das richtige Feld für mich ist und sie gab mir die Gelegenheit, diesen Traum zu ermöglichen.

Ein besonderer Dank geht an Prof. Dr. Andreas Reiner, der mich seit meiner Masterzeit begleitet und immer für Fragen, Anregungen, aber auch experimentelle und konzeptionelle Unterstützung zur Verfügung stand.

Ein großer Dank gebührt außerdem Dr. Karl. W. Kafitz, für seine exzellente fachliche Beratung. Es ist sehr schwer auszudrücken, was für eine Bereicherung er für die Arbeit im Instutut ist, aber um es auf einen Punkt zu bringen: Ohne ihn wäre das Experimentieren nicht möglich.

Ich bedanke mich außerdem herzlichst bei Tanja König die es geschafft hat in Gesprächen aufzubauen, zu bekräftigen und auch zu motivieren.

Ein großer Dank geht an Niklas Gerkau und Daniel Ziemens, die „vorherige Generation“, die mit Rat und Tat zur Verfügung stand und in sowohl professionellen, as auch in persönlichen Situationen ein offenes Ohr hatten.

Ich bedanke mich außerdem bei den Mitgliedern unseres Instituts Jan, Simone, Claudia, Jona, Iris, Sara, Louis und Viola und an die die mich seit der Masterzeit mit begleitet haben und wahre „Doktorinos“ sind: Laura, Sara und Marcel. Ganz besonders möchte ich mich bei meinen Bürokumpanen bedanken… Kathi und Nils… uns verbinden verzweifelte Momente in denen man sich hinterfragt, Momente des Triumpfs und ausgeschlagene Zähne und ich würde nichts daran ändern.

Ich möchte mich vor allen bei meiner Frau Marina bedanken. Wir sind zusammen groß geworden und du hast mich durch die letzen 12 Jahre begleitet, ausgehalten, gefördert und gestärkt. Im Guten und Schlechten (und alles dazwischen) bist du bei mir gestanden und ohne dich hätte ich das nicht geschafft. Ich schätze die Momente, die wir während den letzten Jahren hatten und ich freue mich auf alle Momente, die kommen werden.

Ich möchte mich außerdem bei unseren Familien bedanken. An meine, aber auch an Marinas Eltern, die immer mit einem offenen Ohr zugehört haben und mit Rat und Unterstützung da gewesen sind. An unsere Brüder Ben und Mike auf die man sich immer verlassen konnte, wenn man aus dem wissenschaftler Alltag herausgeholt werden musste.

11. Declaration/ Eidesstattliche Erklärung

Ich versichere an Eides Statt, dass die vorliegende Dissertation von mir selbständig und ohne unzulässige fremde Hilfe unter Beachtung der „Grundsätze zur Sicherung guter wissenschaftlicher Praxis an der Heinrich-Heine-Universität Düsseldorf“ erstellt worden ist. Textstellen oder Abbildungen, die wörtlich oder abgewandelt aus anderen Arbeiten stammen, habe ich mit einer Quellenangabe versehen. Diese Arbeit wurde weder vollständig noch in Teilen einem anderen Prüfungsamt zur Erlangung eines akademischen Grades vorgelegt.

Joel S. E. Nelson Düsseldorf